

Article

The Gold–Palladium Ozernoe Occurrence (Polar Urals, Russia): Mineralogy, Conditions of Formation, Sources of Ore Matter and Fluid

Valery Murzin ¹, Galina Palyanova ^{2,*}, Tatiana Mayorova ³ and Tatiana Beliaeva ²

¹ Zavaritsky Institute of Geology and Geochemistry, Ural Branch of Russian Academy of Sciences, Akademika Vonsovskogo Str., 15, 620016 Ekaterinburg, Russia; murzin@igg.uran.ru

² Sobolev Institute of Geology and Mineralogy, Siberian Branch of Russian Academy of Sciences, Akademika Koptuyuga Pr., 3, 630090 Novosibirsk, Russia; zhur0502@igm.nsc.ru

³ Institute of Geology, Federal Research Center, Komi Science Center, Ural Branch, Russian Academy of Sciences, Pervomaiskaya Str., 54, 167982 Syktyvkar, Russia; mayorova@geo.komisc.ru

* Correspondence: palyan@igm.nsc.ru

Abstract: We studied the mineralization and sulfur isotopic composition of sulfides of gold–palladium ores in olivine clinopyroxenites from the Dzelyatyshor massif made up of a continuous layered series of rocks: olivine-free clinopyroxenite–olivine clinopyroxenite–wehrlite. The primary igneous layering of rocks, manifested as different quantitative ratios of clinopyroxene and olivine in them, controls the local trends of variability in the chemistry of mineral-forming medium and the concentrations of ore components, including noble metals, and sulfur in each separate layer during its cooling. The replacement of primary rock-forming minerals by secondary minerals, when the temperature decreases, is a characteristic trend for pyroxenites: (a) olivine → serpentine, secondary magnetite, and (b) clinopyroxene → amphibole, secondary magnetite → chlorite. The deposition of native gold in parageneses with PGM and sulfides at the Ozernoe occurrence took place during the replacement of earlier rock-forming minerals by chlorite. This process completed mineral formation at the deposit and took place at temperatures 150–250 °C and at the high activity of S, Te, Sb, and As of fluid. The variability of mineral formation conditions during chloritization is reflected in the change of native-sulfide forms of Pd by arsenide-antimonide forms and the sulfur isotopic composition of sulfides. The Pd content in native gold increases in the series—Au–Ag solid solution (<1.5 wt.% Pd)—Au–Cu intermetallides (to 6 wt.% Pd)—Cu–Au–Pd solid solutions (16.2–16.9 wt.% Pd). The sulfur isotopic composition of pyrite, chalcopyrite, and bornite varies from –2.1 to –2.9‰. It is assumed that a deep-seated magmatic basic melt was the source of fluid, ore components, and sulfur.

Keywords: clinopyroxenites; palladium gold; platinum group minerals; chlorite geothermometer; sulfur isotopic composition



Citation: Murzin, V.; Palyanova, G.; Mayorova, T.; Beliaeva, T. The Gold–Palladium Ozernoe Occurrence (Polar Urals, Russia): Mineralogy, Conditions of Formation, Sources of Ore Matter and Fluid. *Minerals* **2022**, *12*, 765. <https://doi.org/10.3390/min12060765>

Academic Editor: Liqiang Yang

Received: 29 April 2022

Accepted: 14 June 2022

Published: 16 June 2022

Publisher's Note: MDPI stays neutral with regard to jurisdictional claims in published maps and institutional affiliations.



Copyright: © 2022 by the authors. Licensee MDPI, Basel, Switzerland. This article is an open access article distributed under the terms and conditions of the Creative Commons Attribution (CC BY) license (<https://creativecommons.org/licenses/by/4.0/>).

1. Introduction

The object of this study is the gold–palladium Ozernoe occurrence at the Dzelyatyshor wehrlite–pyroxenite massif in the Polar Urals (Russia). The massif is situated 80 km southwest of the town of Labytnangi in the upper reaches of the Dzelyatyshor stream, left inflow of the Malaya Kharamatalou river. In its geologic, petrographic, and mineralogic-geochemical features, this occurrence is most similar to the so-called “Baronsky” type of gold–palladium mineralization identified among the Uralian deposits [1]. The typical properties of this type of mineralization are: (1) occurrence in olivine pyroxenites of differentiated clinopyroxenite–gabbro massifs with titanomagnetite mineralization; (2) uneven dispersed impregnation of noble metals in rocks at extremely low contents of associated sulfides and (3) absence of visible changes in the appearance or composition of rocks of ore zones, which are outlined only on the basis of sampling results. In

the world literature, similar mineralization in the rocks of basic-ultrabasic composition is described as poorly sulfidic with a high content of PGE—«low-S-high platinum-group element deposits» [2–4].

A typical object of “Baronsky” type is the Baron–Klyuevo occurrence at the Volkovsky massif in the Middle Urals (Russia). It occurs in the upper differentiated magmatic sections of this massif in the rocks of dunite-clinopyroxenite-gabbro association. Zones with impregnated mineralization ($\text{Pd} > \text{Au} > \text{Pt}$, 0.02–0.04 wt.% S) are localized in olivinites, clinopyroxenites, and olivine–anorthite gabbro that smoothly pass into each other in the southern margin of the massif [1,5,6]. Gold–palladium mineralization at the Baronsky occurrence consists of two spatially separated mineral associations: (1) sulfide, with predominant vysotskite PdS , and (2) arsenide–antimonide, with predominant isomertieite $\text{Pd}_{11}\text{Sb}_2\text{As}_2$ [6,7].

The geologic setting of the Ozernoe occurrence at the Dzelyatyshor massif, petrographic and petrochemical characteristics, and mineralogic-geochemical features of rocks and gold–palladium mineralization were reported in previous studies [8–11]. In this study, we conducted a detailed analysis of the mineral composition and mineral parageneses of gold–palladium ores from the Ozernoe occurrence and obtained the first data on the deposition temperature of noble metal minerals, using the chlorite geothermometer, studied the sulfur isotopic composition of sulfides, determined the sources of ore matter and fluid, and revealed the features of the distribution of Pd and Cu in native gold.

2. Brief Description of the Study Area

In the geological aspect, the Dzelyatyshor massif is surrounded by the Voykar–Synya dunite–harzburgite ophiolite massif, which occurs in the polar part of the Main Uralian fault zone (Figure 1). The rocks of the northeastern framing of this massif belong to the Karshor peripheral striped dunite–wehrlite–clinopyroxenite–gabbro complex, whose age is determined as Late Ordovician [12]. In the southeast, the Karshor complex borders granitoids of the Sobsky granodiorite–tonalite complex (D_{1-2}).

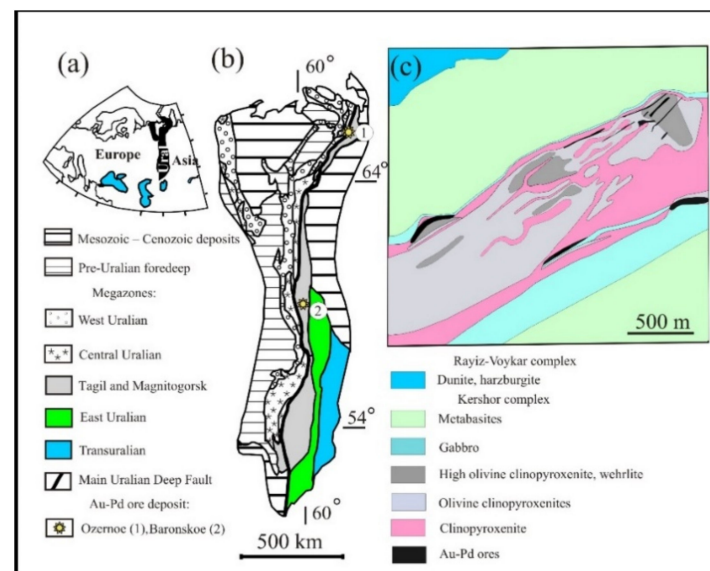


Figure 1. (a) Geographic location of the Urals on the Europe–Asia border; (b) position of Baronsky type objects in the tectonic structures of the Urals (modified from [13]) (on the right); (c) geologic structure and setting of gold–palladium mineralization at the Dzelyatyshor massif.

Clinopyroxenite bodies hosting gold–palladium mineralization of the Ozernoe occurrence were initially attributed to the Karshor complex. In terms of the most modern concepts [10], these clinopyroxenites are identified in the Dzelyatyshor wehrlite–clinopyroxenite massif which is isolated from the Karshor complex. In the petrochemical

characteristics, the Dzelyatyshor massif is similar to the wehrlite–clinopyroxenite series of the Platinum-bearing Belt of the Urals and possesses the features of layering displayed in the replacement of olivine by non-olivine rocks from bottom to top. Its contacts with hosting gabbroids of the Karshor complex are tectonic. The Dzelyatyshor massif is composed of a continuous layered series of rocks—non-olivine clinopyroxenite–olivine clinopyroxenite wehrlite [10]. Mineralization belongs to the poor sulfide stratiform type and tends to sheet-like bodies of olivine clinopyroxenites in the upper part of the massif. The bodies consist of 13 ore bodies from 2 to 30 m in thickness [10]. The content of metals in the ores, determined using atomic absorption spectrometry, are: 1.5 wt.% Cu, 2.9 ppm Au, 3.7 ppm Pd, and 1.0 ppm Pt [9,10].

Noble metal mineralization is localized at two levels within the massif. The first lower level occurs in the near-contact part of the massif. The second upper ore level occurs on the horizon of high-olivine pyroxenites with layers of wehrlite. The ore-bearing rocks contain impregnation of magnetite (to 5–7%) and hypogene sulfides, among which chalcopyrite, bornite, pyrrhotite, and pentlandite are predominant. The content of sulfides is typically less than 0.5%, to 1–3% in some parts. Among ores, we identified primary late magmatic minerals, forming segregations of interstitial, and secondary minerals in the form of veinlets and segregations of various shapes, associated with secondary silicates, mainly with serpentine [10].

Noble metal minerals, which amount to 30, are commonly associated with sulfides. The contents of Au and Ag directly correlate with copper content. Geochemical and spatial distribution of the early platinum–metal and later gold–copper mineralization is observed [10].

3. Samples and Research Methods

We studied the samples of olivine-bearing clinopyroxenites with elevated contents of Au and Pd (1–2 ppm), collected from near-surface mine workings (ditches 101, 108, and 126), driven while prospecting for gold by the JSC Yamal Mining Company in 2008. The rocks consist of coarse-grained varieties with olivine content from 1 to 10–15% and with grain sizes of main minerals from 1 to 15 mm. Ore minerals in clinopyroxenites are represented by dispersed impregnations of fine (less than 0.1 mm) and enlarged (to 2–3 mm) magnetite, and sulfides with grain sizes less than 0.5 mm. The content of magnetite in all samples is commonly no more than 2–3%, and that of sulfides is less than 0.5%. In rare cases, the amount of sulfides was 10%, and their grain sizes were more than 2 mm.

The studied samples of clinopyroxenites were separated into three groups according to the content of olivine and sulfides as well as to predominant minerals in sulfide parageneses (Table 1, Figure 2). Sulfides in clinopyroxenites I–III were attributed by us to pyrite–pyrrhotite–chalcopyrite, bornite–chalcopyrite and pyrrhotite–chalcopyrite–pyrite parageneses, respectively. Clinopyroxenites I and III are similar in the specific composition of sulfides, but differ in the content and quantitative ratios of the main sulfide minerals. Clinopyroxenites II and III are characterized by an association of sulfides with magnetite, the crystals of which are enclosed in sulfides or form rims on sulfide segregations (Figure 2c,d).

Table 1. Features of studied clinopyroxenite samples from Ozernoe occurrence.

Samples of Groups	No Sample	Trench Exploration Nor	Olivine Content, Vol. %	Sulfide Content, Vol. %	Sulfide Parageneses
clinopyroxenite I	1545, 1546	K-108, 126	<5	<0.1	Py >> Pyh > Ccp
clinopyroxenite II	101012, 101013	K-101	5–10	0.1–0.5	Bn-Ccp
clinopyroxenite III	211014, 211015	P2110, K-104	>10–15	<10	Pyh > Ccp > Py

Note. Minerals: Py—pyrite, Pyh—pyrrhotite, Ccp—chalcopyrite, Bn—bornite. Abbreviations of minerals are given following the recommendation of IMA [14].

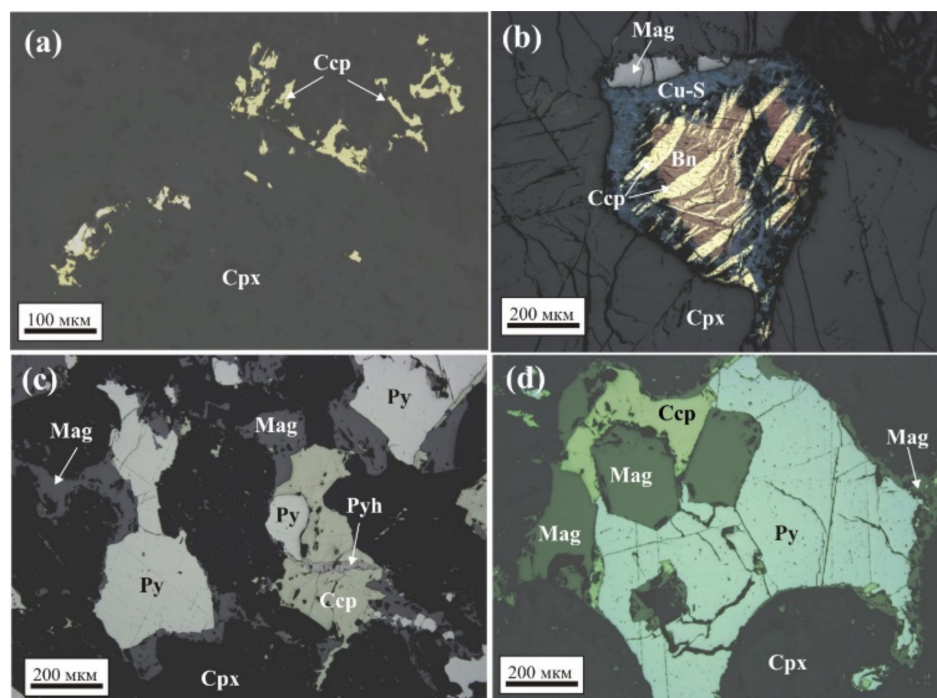


Figure 2. Relationships of main ore minerals in the samples of clinopyroxenites I (a), II (b), and III (c,d). Bn—bornite, Ccp—chalcocopyrite, Cpx—clinopyroxene, Cu-S—secondary copper sulfide, Mag—magnetite, Py—pyrite, Pyh—pyrrhotite.

Microprobe analyses of minerals of clinopyroxenites I and II were carried out with a CAMECA SX-100 equipped with five WDS spectrometers and a Bruker energy dispersive spectrometer system at the Common Use Center “Geoanalyst” of the Institute of Geology and Geochemistry, Ural Branch of the Russian Academy of Sciences (Ekaterinburg, Russia). Quantitative WDS analyses were performed at 25 kV accelerating voltage and 20 nA sample current, with a beam diameter of about 1 μm .

Analysis of the polished sections of clinopyroxenites III was performed on the scanning electron microscope Tescan Vega 3LMN (Tescan, Czech Republic) with an energy dispersive spectrometer X-Max 50 (Oxford Instruments, Oxford, UK) in the Institute of Geology KomiSC UB of the RAS. Analytical conditions: accelerating voltage was 20 kV, beam current was 15 nA, with the beam diameter up to 1 μm .

Isotopic mass-spectrometric analysis of sulfide sulfur of clinopyroxene II was conducted in the Laboratory of Stable Isotopes in the FEGI FEB RAS. The samples were prepared by laser method using the NWR Femto femtosecond laser ablation [15,16]. The ratio of sulfur isotopes was measured on the MAT-253 mass-spectrometer (Thermo Fisher Scientific, Dreieich, Germany) relative to the laboratory working standard calibrated according to international standards IAEA-S-1, IAEA-S-2 и IAEA-S-3. Results of measurements of $\delta^{34}\text{S}$ are reported relative to the international standard VCDT and are given in ppm (‰). The accuracy of analysis was $\pm 0.2\text{‰}$ (2σ).

The classification of amphiboles is based on the scheme from [17] and that of pyroxenes, on the classical scheme from [18]. The temperature regime of deposition of noble metal minerals was performed using data for chlorite geothermometer, based on the amount of tetrahedral aluminum (Al^{IV}) and molar fraction of iron X_{Fe} by the formula $T, ^\circ\text{C} = 17.5 + 106.2 \times (\text{Al}^{\text{IV}} - 0.88 \times [X_{\text{Fe}} - 0.34])$ [19].

4. Results

4.1. Mineralogy, Mineral Association, and Sequence of Mineral Formation at the Ozernoe Occurrence

4.1.1. Primary (Early) Rock-Forming Minerals of Clinopyroxenites

1. Clinopyroxene

- Primary clinopyroxene with grain sizes from 0.1 to 10 mm in the samples of all groups of clinopyroxenites belongs to the diopside-hedenbergite with a varying ferrosilite mineral (Figure 3a). In clinopyroxenites I and II, it corresponds to diopside with an elevated content of FeO (4.47–7.04 wt.%) and Al₂O₃ (0.79–2.74 wt.%) (Table 2). It contains minor Ti, Mn, Cr, and Na in amounts less than 1 wt.%. Clinopyroxene in clinopyroxenite III is also represented by diopside but with lower contents of FeO (0.66–2.17 wt.%), Al₂O₃ (less than 1.7 wt.%), and other trace elements. This clinopyroxene also contains the thinnest plates of iron oxide, supposedly magnetite, which develop along cleavage cracks (Figure 4a). These plates seem to be the result of the decomposition of the solid solution or oxidation of Fe²⁺.

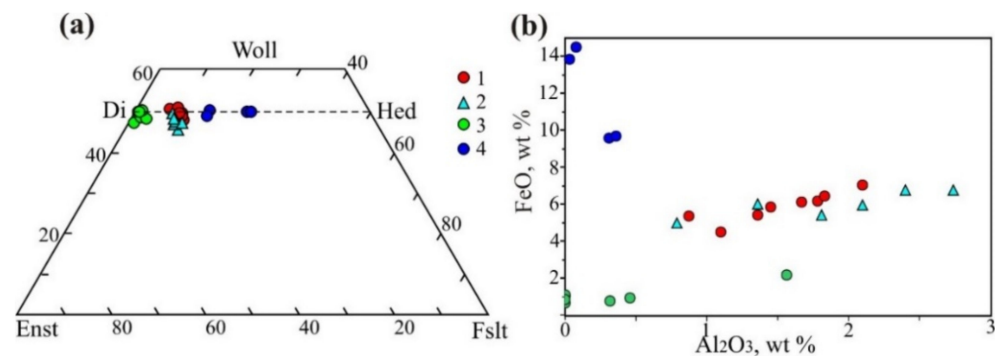


Figure 3. Diagrams of composition of clinopyroxenes (a) and contents of FeO–Al₂O₃ (b) in primary and secondary clinopyroxenites. Primary clinopyroxene from clinopyroxenites I (1), II (2), and III (3). 4—secondary clinopyroxene from clinopyroxenite I.

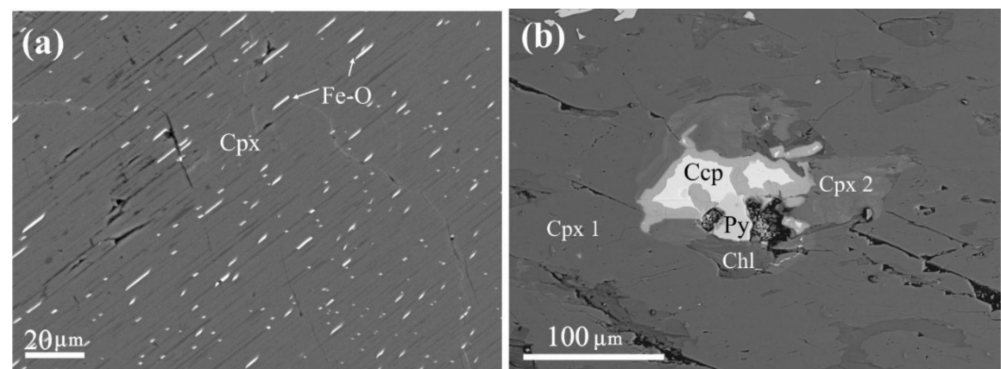


Figure 4. Clinopyroxene in samples of clinopyroxenites III (a) and I (b). (a) Thin plates of Fe–O phase in primary clinopyroxene (Cpx); (b) secondary clinopyroxene (Cpx 2) in intergrowths with chlorite (Chl), pyrite (Py), and chalcopyrite (Ccp) in primary clinopyroxene (Cpx 1).

- In spite of considerable variations in the composition of primary clinopyroxene, clinopyroxenites I–III have a direct correlation with the contents of FeO and Al₂O₃ (Figure 3b). An inverse correlation dependence was revealed only for clinopyroxene grains with the highest iron content (Figure 3b, sign 4) (Table 2, No. 9–12). We attributed this clinopyroxene to a later generation. Along with sulfides and chlorite, it fills interstices in the aggregates of early primary pyroxene grains (Figure 4b).

Table 2. Chemical composition of clinopyroxenes in clinopyroxenites I–III (in wt.%).

No	Sample #	SiO ₂	TiO ₂	Al ₂ O ₃	Cr ₂ O ₃	FeO *	MnO	MgO	CaO	Na ₂ O	Total
1	1545-2-3	52.68	0.14	1.36	b.d.	5.44	0.25	14.78	25.17	0.14	99.96
2	1545-2-12	52.13	0.16	1.78	b.d.	6.2	0.2	14.44	24.73	0.06	99.70
3	1545-2-14	51.02	0.14	1.67	0.12	6.11	0.21	14.43	23.87	0.09	97.66
4	1545-2-18	52.83	<i>0.04</i>	1.1	<i>0.02</i>	4.47	0.16	15.36	25.6	0.07	99.65
5	1545-1-35	52.31	0.15	2.1	0.06	7.04	0.11	14.37	23.73	0.06	99.93
6	1545-1-45	51.85	0.1	1.83	b.d.	6.45	0.16	14.11	23.88	0.16	98.54
7	1546-3-8	53.4	0.1	0.87	0.13	5.34	0.16	14.29	25.16	0.11	99.56
8	1546-3-13	53.45	<i>0.11</i>	1.45	b.d.	5.84	0.26	14.44	24.46	<i>0.05</i>	100.06
9	1546-3-5	52.1	0.01	b.d.	0.01	13.77	1.25	9.21	24.31	<i>0.03</i>	100.69
10	1546-3-7	52.08	0.04	0.08	0.04	14.51	0.62	8.78	24.16	<i>0.04</i>	100.35
11	1546-3-6	52.91	0.01	0.31	0.09	9.56	0.26	11.92	24.58	0.17	99.81
12	1545-1-41	52.59	<i>0.09</i>	0.36	0.03	9.67	0.32	11.98	23.36	1.16	99.56
13	101013-24	51.74	<i>0.18</i>	2.74	<i>0.12</i>	6.77	0.22	14.8	21.97	0.34	98.88
14	101013-27	53.45	<i>0.09</i>	1.36	<i>0.04</i>	6.02	0.15	15.41	23.4	0.08	100.00
15	101013-33	54.27	<i>0.02</i>	0.79	b.d.	4.98	<i>0.12</i>	15.2	24.79	<i>0.04</i>	100.21
16	101012-39	53.34	<i>0.16</i>	2.1	<i>0.07</i>	5.98	<i>0.11</i>	15.07	23.52	0.1	100.45
17	101012-48	51.6	0.27	2.4	<i>0.1</i>	6.77	0.16	14.2	22.67	0.1	98.27
18	101012-57	52.4	<i>0.09</i>	1.81	<i>0.01</i>	5.42	0.25	14.72	23.38	0.09	98.17
19	211015-1_3	55.5	b.d.	b.d.	b.d.	1.04	b.d.	18.68	25.57	b.d.	100.79
20	211015-2_6	55.21	b.d.	b.d.	b.d.	0.66	b.d.	18.35	25.86	b.d.	100.08
21	211015-3_3	54.85	b.d.	0.32	b.d.	0.74	b.d.	19.19	24.48	b.d.	99.58
22	211015-4_1	54.31	b.d.	0.46	b.d.	0.93	b.d.	18.61	25.62	b.d.	99.93
23	211015-6_3	54.05	b.d.	1.56	b.d.	2.17	b.d.	17.61	24.47	b.d.	99.86
24	211014-2_2	55.17	b.d.	b.d.	b.d.	1.11	b.d.	18	26.15	b.d.	100.43
25	211014-3_4	55.3	b.d.	b.d.	b.d.	0.85	b.d.	18.23	26.02	b.d.	100.4

Note. Primary clinopyroxene from samples of pyroxenites I (No 1–8), II (No 13–18), and III (No 19–15). No 9–12—secondary clinopyroxene. Here and below in the tables: FeO *—calculated content from measured Fe; definitions with the values of element concentrations below 2 θ (standard error of analysis) are highlighted in italics; «b.d.»—below the detection limit.

2. Olivine

Olivine in the rocks under study is characterized by ferruginous fayalite component $x(\text{Fa})$ within 0.13–0.30. The most ferruginous olivine with $x(\text{Fa}) = 0.25–0.30$ is present in the samples of clinopyroxenite I and II, whereas olivine in clinopyroxenite III contains less iron $x(\text{Fa}) = 0.13–0.15$ (Table 3). A constant trace element in olivine is manganese (0.37–0.53 wt.%).

Table 3. Chemical composition of olivine from clinopyroxenites I–III (in wt.%).

No	Clinopyroxenite I			II		III	
	1	2	3	4	5	6	7
Sample #	1545-2-7	1545-2-30	101012-47	101013-26	211015/6	211015/8	211014/4
SiO ₂	38.34	37.97	38.06	37.79	40.07	40.25	39.96
TiO ₂	b.d.	b.d.	b.d.	<i>0.03</i>	b.d.	b.d.	b.d.
Al ₂ O ₃	0.01	b.d.	b.d.	<i>0.04</i>	b.d.	b.d.	b.d.
Cr ₂ O ₃	b.d.	b.d.	b.d.	<i>0.07</i>	b.d.	b.d.	b.d.
FeO	22.41	23.36	24.82	27.01	13.75	12.34	13.28
MnO	0.43	0.43	0.4	0.37	0.49	0.4	0.53
MgO	38.36	37.8	36.06	34.82	45.43	46.95	46.48
CaO	<i>0.01</i>	0.02	b.d.	0.01	0.01	b.d.	b.d.
Na ₂ O	<i>0.01</i>	b.d.	b.d.	b.d.	b.d.	b.d.	b.d.
K ₂ O	b.d.	b.d.	<i>0.01</i>	b.d.	b.d.	b.d.	b.d.
Σ	99.57	99.58	99.35	100.14	99.75	99.94	100.25
$x(\text{Fo})$	0.75	0.74	0.72	0.70	0.85	0.87	0.87
$x(\text{Fa})$	0.25	0.26	0.28	0.30	0.15	0.13	0.13

- Magnetite

Xenomorphous segregations of primary magnetite to 2–3 in size fill interstices in the aggregates of clinopyroxene grains. Interstitial magnetite contains chains of small spinel inclusions, oriented in several directions, and rare plates of ilmenite and in some cases is rimmed by secondary silicates—amphibole (magnesian-hornblende) or chlorite. Interstitial magnetite is represented by the Cr-Ti-V-bearing variety. The content of Cr₂O₃ in it attains 2.9 wt.%, TiO₂—2.5 wt.%, V₂O₃—1.1 wt.% (Table 4, # 1–6). Tabular ilmenite in primary magnetite contains Mg (1.66 wt.% MgO), Mn (3.9 wt.% MnO), and V, Cr, Al in amounts less than 0.2 wt.%.

Table 4. Chemical composition of primary interstitial magnetite in clinopyroxenites I and II (in wt.%).

No	# Sample	No. Grain	FeO *	Cr ₂ O ₃	TiO ₂	Al ₂ O ₃	MgO	MnO	V ₂ O ₃	Total
I	1	1545-2-19	89.8	2.53	0.61	0.52	0.14	0.1	0.94	94.64
	2	1545-2-26	89.16	2.21	0.77	0.11	0.44	0.16	0.85	93.70
	3	1545-1-36	87.25	1.57	2.46	1.35	0.25	0.15	0.94	93.97
	4	101013-22	87.21	2.89	2.16	1.64	0.16	0.21	0.74	95.01
II	5	101013-23	87.17	2.78	2.44	0.99	0.06	0.14	1.05	94.63
	6	101012-49	87.79	2.36	1.74	0.56	0.47	0.21	0.91	94.04

4.1.2. Secondary (Late) Minerals in Clinopyroxenites

Secondary clinopyroxenite minerals are chlorite, serpentine, magnetite, and sulfides, as well as accessory clinopyroxene, titanite, and noble metal minerals. These minerals are present in small quantities (no more than 5–10% in total) and are evenly distributed in the rock mass. Secondary minerals occur in the most permeable zones of granular aggregates of rock-forming minerals. They develop along the cleavage cracks of clinopyroxene, fill microcracks in olivine or clinopyroxene, and are localized in the interstices in olivine–clinopyroxene aggregates.

- Secondary clinopyroxene

Secondary clinopyroxene was observed in clinopyroxene I in single cases. It occurs in association with sulfides (pyrite, chalcopyrite) and chlorite, which fill interstices in the aggregates of primary clinopyroxene grains (Figure 4b). Secondary clinopyroxene in comparison with primary clinopyroxene has a higher iron content (9.6–14.5 wt.% FeO) and a low alumina concentration (less than 0.4 wt.% Al₂O₃) (Figure 3b; Table 2, No 9–12).

- Amphibole

In the samples of clinopyroxenites I and II, amphiboles belong to the group of Ca-amphiboles. They consist of actinolite (No 1–6), magnesian-ferri-hornblende (No 7), magnesian-hornblende (No 8–14), and tremolite (No 15, 16) (Table 5). All amphiboles, except tremolite, contain minor amounts of sodium (from 0.4 to 1.5 wt.% Na₂O) and titanium (to 0.5 wt.% TiO₂) (Table 5). Tremolite contains the least amount of Al₂O₃ and FeO among amphiboles.

Actinolite is developed mainly in the samples of clinopyroxenite I in the form of angular interstitial segregations in the aggregate of clinopyroxene grains (Figure 5a). It is accompanied by small (less than 10 μm) grains of impurity-free secondary magnetite. We have also detected a grain of magnesian-ferri-hornblende virtually completely replaced by chlorite (Figure 6c). Magnesian-hornblende is developed predominantly in clinopyroxenite II in which it, together with chlorite, forms rims on the segregations of primary magnetite and a lattice-like chalcopyrite–bornite aggregate in the interstices of clinopyroxene (Figure 5b). Tremolite is present in all clinopyroxenite samples. It is developed along with the contacts of large clinopyroxene and olivine grains. In the contact zone of these minerals, clinopyroxene is replaced by tremolite, and olivine, by serpentine. Along with tremolite and serpentine, secondary magnetite is formed as symplectic intergrowths with tremolite and larger porous

segregations in serpentine (Figure 5c,d). Tremolite and serpentine in clinopyroxene II replace marginal parts of lattice-like bornite–chalcopyrite segregations.

Table 5. Chemical composition of amphiboles in clinopyroxenites I (No 1–5, 7, 14, 16) and II (No 6, 8–13, 15) (in wt.%).

No	Sample #	SiO ₂	Al ₂ O ₃	Na ₂ O	MgO	F	Cl	K ₂ O	CaO	TiO ₂	FeO *	MnO	Cr ₂ O ₃	Total
1	1546-3-9	50.54	6.1	0.96	16.38	0.07	0.03	0.03	13.16	0.17	9.59	0.16	0.13	97.31
2	1546-3-16	51.26	5.01	0.71	16.33	0.09	0.04	0.08	12.43	0.22	10.32	0.16	0.2	96.85
3	1546-3-19	50.85	5.84	1.05	17.52	0.03	0.33	0.01	12.53	0.36	8.01	0.2	0.16	96.91
4	1546-3-20	52.28	5.09	0.63	17.34	0.05	0.03	0.03	12.88	0.28	8.54	0.12	0.2	97.48
5	1546-3-21	53.83	4.23	0.39	18.77	н.о	0.02	0.01	13.00	0.18	6.94	0.14	0.06	97.57
6	101013-31	53.88	4.51	0.59	19.34	н.о	0.03	0.11	13.01	0.13	6.04	0.15	н.о	97.8
7	1546-3-15	47.67	8.12	0.9	15.28	0.15	0.08	0.14	11.48	0.45	12.68	0.24	0.24	97.45
8	101013-32	47.19	10.35	1.4	16.48	0.06	0.03	0.26	12.63	0.48	8.45	0.11	0.25	97.68
9	101012-45	49.05	9.59	1.37	16.82	0.03	0.01	0.01	12.21	0.52	7.11	0.08	0.14	96.95
10	101012-46	48.58	8.68	1.33	16.87	0.08	0.02	н.о	12.24	0.49	8.27	0.1	0.1	96.77
11	101013-25	51.11	7.35	1.08	17.89	0.07	0.02	0.05	12.28	0.28	7.47	0.1	0.05	97.76
12	101012-55	48.67	9.32	1.28	17.11	0.07	0.02	0.04	12.33	0.37	7.46	0.04	0.12	96.83
13	101012-56	48.5	9.82	1.53	17	0.04	0.03	0.03	12.35	0.38	7.63	0.1	0.05	97.45
14	1545-2-4	48.78	7.55	1.01	18.07	н.о	0.01	0.07	12.5	0.35	8.01	0.12	0.06	96.52
15	101012-42	57.72	0.02	b.d.	22.7	0.02	н.о	0.01	13.22	0.07	2.65	0.03	н.о	96.44
16	1545-2-5	56.1	1.14	0.19	22.22	н.о	0.01	0.02	12.96	0.08	3.82	0.17	н.о	96.7

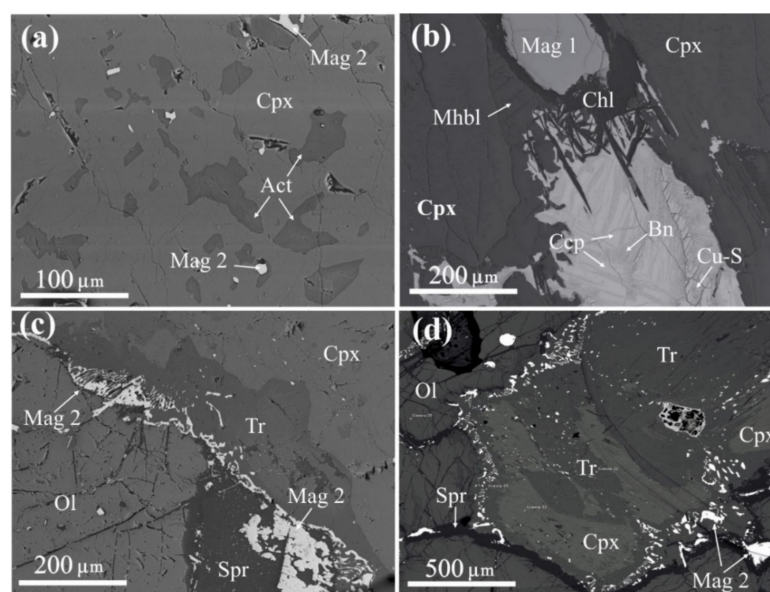


Figure 5. Amphibole in the samples of clinopyroxenite I (a,c), II (b), and III (d). (a) Interstitial segregations of actinolite (Act) in clinopyroxene (Cpx) and associated grains of secondary magnetite (Mag 2); (b) magnesio–hornblende (Mhbl) and chlorite (Chl) in the rim of primary magnetite segregations (Mag 1); aggregate of bornite (Bn), chalcopyrite (Ccp), and secondary copper sulfide (Cu-S) in clinopyroxene matrix (Cpx); (c,d) development of tremolite (Tr), serpentine (Spr) and secondary magnetite (Mag 2) in the contact zone of clinopyroxene (Cpx) and olivine (Ol).

- Chlorite

In clinopyroxenites I and II, chlorite is developed in the interstices of clinopyroxene (Figure 6a) or along cutting microcracks (Figure 6b). Chlorite replaces primary clinopyroxene, magnesio-ferri-hornblende (Figure 6c), and magnetite (Figure 6d). Tabular chlorite in clinopyroxenite II together with tremolite and serpentine are developed in the marginal parts of segregations of bornite–chalcopyrite lattice-like aggregate (Figure 5b). A typical fea-

ture of chlorite in clinopyroxene I is the presence of titanite (Figure 6c,d). In clinopyroxenite III, chlorite is distributed mainly along the cleavage cracks of clinopyroxene.

In the chemical composition, chlorite corresponds to pennine and pycnochlorite and is characterized by wide variations in iron content (Figure 7). Chlorite in clinopyroxenite I has the highest iron concentration $X_{Fe} = 0.1$ – 0.43 compared to chlorite in clinopyroxenite II and III ($X_{Fe} < 0.1$) (Table 6). Chlorite with the lowest iron concentration ($X_{Fe} < 0.05$) was found in clinopyroxenite III. Only in these samples chlorite (pennine) contains minor amounts of potassium (0.5–2 wt.% K_2O).

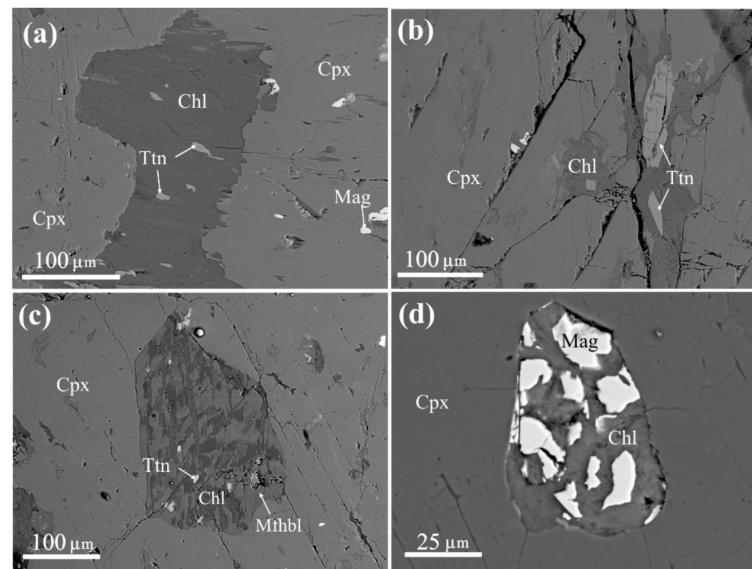


Figure 6. Chlorite in the samples of clinopyroxene I. (a) Interstitial chlorite (Chl) in clinopyroxene (Cpx). Chlorite also contains titanite (Ttn) and magnetite (Mag) in clinopyroxene; (b) veinlets of chlorite (Chl) with inclusions of titanite (Ttn) in clinopyroxene; (c) segregation of magnesio-ferri-hornblende (Mfhbl) in clinopyroxene. Amphibole is replaced by chlorite with titanite inclusions (Ttn); (d) magnetite crystal (Mag) replaced by chlorite (Chl) in clinopyroxene.

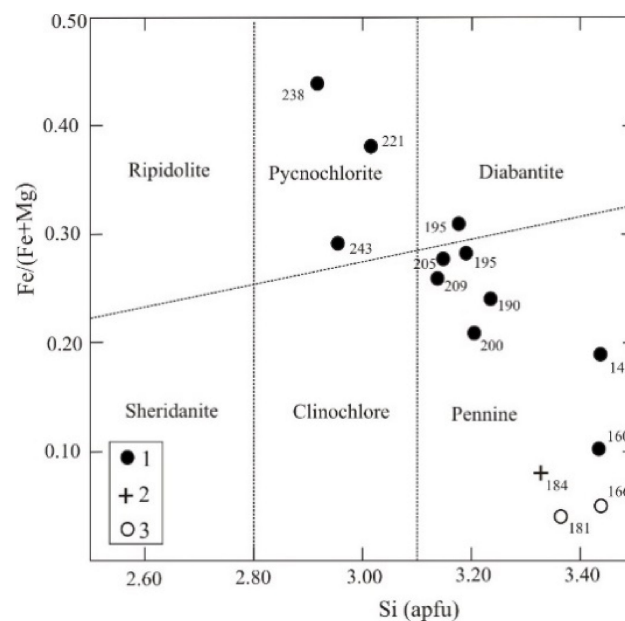


Figure 7. Chlorite composition on the classification diagram from [20]. Analyses of chlorite from clinopyroxenites I (1), II (2), and III (3). Numbers show the formation temperatures calculated with a chlorite geothermometer [19] (Table 6).

Table 6. Chemical composition of chlorite from clinopyroxenites I–III (in wt.%) and calculated temperatures of its formation.

No Grain	1545-2-2	1545-2-13	1545-2-17	1545-2-21	1545-2-22	1545-2-25	1545-1-34	1545-1-39	1545-1-44	1546-3-10	1546-3-17	101012-54	211015/4_2	211014/2_3
No	1	2	3	4	5	I 6	7	8	9	10	11	II 12	13	III 14
SiO ₂	30.67	31.63	31.59	30.71	35.12	28.65	34.51	27.18	30.96	28.81	30.61	33.82	34.87	35.94
TiO ₂	b.d.	b.d.	b.d.	b.d.	b.d.	b.d.	b.d.	b.d.	b.d.	b.d.	b.d.	b.d.	b.d.	0.23
Al ₂ O ₃	13.88	13.61	14.03	15.09	11.75	15.39	10.76	17.53	13.9	17.93	14.21	14.32	12.85	12.18
Cr ₂ O ₃	0.51	0.21	0.68	0.11	0.03	0.16	0.45	0.28	0.1	0.05	0.64	0.19	0.14	b.d.
FeO	16.53	13.63	12.13	14.84	6.02	21.29	11.76	23.09	16.35	16.36	17.69	5.05	2.69	3.11
MnO	0.1	0.12	0.16	0.26	0.08	0.17	0.41	0.21	0.21	0.25	0.2	0.03	b.d.	b.d.
MgO	24.33	25.69	26.69	24.63	32.25	20	28.24	17.07	24.02	22.38	22.4	31.15	34.04	32.97
CaO	0.03	0.11	0.07	0.05	0.06	0.1	0.14	0.08	0.02	0.12	0.1	0.06	b.d.	b.d.
Na ₂ O	b.d.	b.d.	b.d.	b.d.	b.d.	b.d.	b.d.	b.d.	b.d.	b.d.	b.d.	b.d.	b.d.	b.d.
K ₂ O	b.d.	b.d.	b.d.	b.d.	b.d.	b.d.	b.d.	b.d.	b.d.	b.d.	b.d.	b.d.	0.54	2.10
Σ	86.05	85.00	85.35	85.69	85.31	85.76	86.27	85.44	85.56	85.90	85.85	84.62	85.13	86.53
Crystallochemical coefficients in the chlorite formula (calculation for 20 cations)														
Si	6.29	6.47	6.40	6.27	6.87	6.05	6.91	5.84	6.38	5.92	6.36	6.66	6.72	6.86
Ti	0.00	0.00	0.00	0.00	0.00	0.00	0.00	0.00	0.00	0.00	0.00	0.00	0.00	0.03
Al	3.35	3.28	3.35	3.63	2.71	3.83	2.54	4.44	3.38	4.34	3.48	3.32	2.92	2.74
Cr	0.08	0.03	0.11	0.02	0.00	0.03	0.07	0.05	0.02	0.01	0.11	0.03	0.02	0.00
Fe ^{III}	0.00	0.00	0.07	0.00	0.00	0.13	0.00	0.00	0.00	0.00	0.01	0.00	0.00	0.00
Fe ^{II}	2.83	2.33	1.98	2.53	0.98	3.63	1.97	4.14	2.81	2.81	3.05	0.83	0.43	0.50
Mn	0.02	0.02	0.03	0.04	0.01	0.03	0.07	0.04	0.04	0.04	0.04	0.01	0.00	0.00
Mg	7.43	7.83	8.05	7.49	9.40	6.29	8.42	5.47	7.37	6.85	6.93	9.14	9.77	9.37
Ca	0.01	0.02	0.02	0.01	0.01	0.02	0.03	0.02	0.00	0.03	0.02	0.01	0.00	0.00
Na	0.00	0.00	0.00	0.00	0.00	0.00	0.00	0.00	0.00	0.00	0.00	0.00	0.00	0.00
K	0.00	0.00	0.00	0.00	0.00	0.00	0.00	0.00	0.00	0.00	0.00	0.00	0.13	0.51
x(Mg)	0.72	0.77	0.80	0.74	0.90	0.63	0.81	0.57	0.72	0.71	0.69	0.92	0.96	0.95
Al(IV)	1.71	1.53	1.60	1.73	1.13	1.95	1.09	2.16	1.62	2.08	1.64	1.34	1.28	1.14
Al(VI)	1.64	1.76	1.75	1.90	1.58	1.88	1.44	2.28	1.76	2.26	1.84	1.98	1.64	1.59
x(Fe)	0.28	0.23	0.21	0.26	0.10	0.38	0.19	0.43	0.28	0.29	0.31	0.08	0.04	0.05
T, °C	205	190	200	209	160	221	147	238	195	243	195	184	181	166

Note. In calculating crystallochemical formula, Al(IV) supplements Si position to 8 cations, and Al(VI) accounts for the rest part of the total calculated amount of Al.

- Serpentine

In all samples of clinopyroxenites, serpentine actively replaces olivine through the net of microcracks (Figure 8a,b). Among two types of serpentinites are distinguished according to morphology and chemical composition: A (coarse-lamellar, supposedly antigorite) and B (fibrous, apparently lizardite). Serpentine A is developed in clinopyroxenites I and II. Serpentine B is present in clinopyroxenite III. Serpentine A replaces the most ferruginous olivine (22.4–27.9 wt.% FeO) (Table 3, No 1–4) and, in turn, contains the highest iron content (4.6–12.8 wt.% FeO) (Table 7, No 1–5). Serpentine B is less ferruginous (1.1–2.2 wt.% FeO) (Table 7, No 6–10) than serpentine A and replaces olivine with a lower iron content (12.3–13.8 wt.% FeO) (Table 3, No 5–7) $X(\text{Fa}) = 0.13\text{--}0.15$ (Table 3, No 6–10). Coarse grains of porous secondary magnetite, tremolite and chalcopyrite are deposited in olivine together with serpentine A (Figure 8b). Serpentine A also corrodes primary magnetite grains and forms symplectic intergrowths with secondary magnetite (Figure 8a). In clinopyroxenite II, serpentine A is developed at the contacts of olivine and clinopyroxene grains. Here, together with tremolite, it is present in the marginal parts of sulfide segregations of bornite–chalcopyrite paragenesis (Figure 8c). In clinopyroxenite III, lamellar (fibrous) aggregates of serpentine B replace pyrite and chalcopyrite grains (Figure 8d).

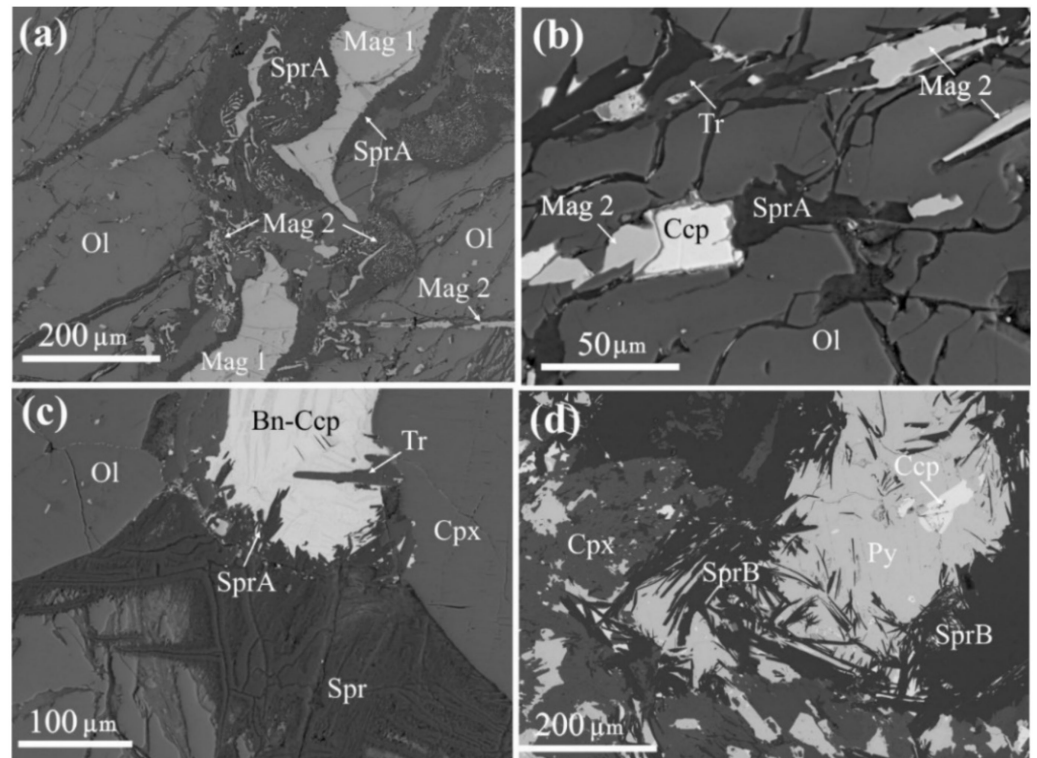


Figure 8. Serpentinite in samples of clinopyroxenites I (a,b), II (c), and III (d). (a) Relationships of serpentine A (Spr A) with primary (Mag 1) and secondary magnetite (Mag 2) in large olivine grain (Ol); (b) microcracks in olivine (Ol) filled with serpentine A (Spr A), tremolite (Tr), chalcopyrite (Ccp), and secondary magnetite (Mag 2); (c) localization of serpentine A (Spr A) and sulfides of bornite–chalcopyrite paragenesis (Bn–Ccp) in interstices of olivine (Ol) and clinopyroxene (Cpx) grains. Serpentine A (Spr A) together with tremolite (Tr) corrodes the marginal part of sulfide segregation; (d) fibrous aggregates of serpentine B (Spr B) corroding the marginal parts of large segregation of pyrite (Py).

Table 7. Chemical composition of serpentine in clinopyroxenites I–III (in wt.%).

	No	# Grain	MgO	FeO	Al ₂ O ₃	SiO ₂	Cr ₂ O ₃	MnO	NiO	Total
I	1	1545-2-55	37.65	4.63	b.d.	44.01	B.d.	B.d.	B.d.	86.29
	2	101013-29	28.91	12.78	0.54	43.47	0.01	0.27	0.05	86.17
	3	101013-30	31.43	7.34	0.01	50.52	0.07	0.06	0.04	89.84
II	4	101012-43	32.86	5.71	0.03	49.76	0.03	0.12	0.04	88.83
	5	101012-44	34.38	6.02	0.02	45.39	0	0.08	0.05	86.17
	6	211015-3_1	39.52	2.15	0.49	44.89	B.d.	B.d.	B.d.	87.05
	7	211015-3_2	39.37	1.18	B.d.	45.08	B.d.	B.d.	B.d.	85.63
III	8	211015-6_2	40.64	1.12	B.d.	45.33	B.d.	B.d.	B.d.	87.1
	9	211015-8_2	40.3	1.25	B.d.	45.61	B.d.	B.d.	B.d.	87.16
	10	211014-4_2	39.63	1.48	B.d.	44.38	B.d.	B.d.	B.d.	85.5

- Secondary magnetite

Secondary magnetite is present in all studied clinopyroxenites in amounts from 0.5 to 5–10%. In clinopyroxene, it consists of grains less than 0.05 mm in size of isometric or angular shape, which are localized in the cleavage cracks of this mineral, occasionally in the intergrowth with interstitial actinolite (Figure 5a). In olivine, thin veinlets or chains of small secondary magnetite grains fill the central part of cracks filled with serpentine (Figure 8a,b). At the contact of large olivine and pyroxene grains, tiny parts of secondary magnetite “are gathered” in larger porous aggregates in serpentine or form symplectic intergrowths with serpentine or tremolite (Figures 5c,d and 8a). Secondary magnetite in clinopyroxenites II and III overgrows interstitial sulfide segregations or, in clinopyroxene III, its crystals are enclosed in pyrite or chalcopyrite (Figure 2b–d). In contrast to primary magnetite with elevated content of Cr, Ti, and V (Table 4), the contents of trace elements in secondary magnetite are lower and, typically, are below the detection limit or error of analysis (Table 8).

Table 8. Chemical composition of secondary magnetite (in wt.%).

No	# Grain	FeO	Cr ₂ O ₃	TiO ₂	Al ₂ O ₃	MgO	MnO	V ₂ O ₃	Total
1	1545-2-9	92.67	b.d.	0.32	0.02	0.15	0.02	0.1	93.28
2	101013-34	92.16	0.44	0.29	0.07	0.16	0.01	0.28	93.41
3	101012-37	90.14	0.63	0.65	0.02	0.1	0.12	0.54	92.20
4	211015_3_9	94.18	b.d.	b.d.	b.d.	b.d.	b.d.	b.d.	94.18
5	211015_5_1	89.89	b.d.	b.d.	b.d.	b.d.	0.37	b.d.	90.26

Note. Samples of clinopyroxenites I (No 1), II (No 3,4) and III (No 5). Analyses: 1,5—in symplectic intergrowths with amphibole; 2—microveinlets in serpentine; 3—inclusion in bornite-chalcopyrite lattice-like aggregate; 4—overgrown on large pyrite segregations.

- Sulfides

In clinopyroxenite I, pyrite, pyrrhotite, and chalcopyrite are in paragenesis with interstitial and veinlet chlorite and are generally typically enclosed in it (Figure 9a–c). Occasionally, sulfide grains are localized in pyroxene but form intergrowths with chlorite (Figure 9d). In clinopyroxenite II, sulfides consisting of decomposed solid solution are localized in the interstices of clinopyroxene grains occasionally together with secondary magnetite (Figure 2b). In the contact zones of olivine and clinopyroxene grains, lattice-like chalcopyrite bornite aggregates in the marginal parts are replaced by tremolite, chlorite and serpentine (Figures 5b and 8c). In clinopyroxenite III, sulfide segregations of interstitial shapes to 2 mm in size are disseminated in the rock mass. Among sulfides, pyrite predominates quantitatively over chalcopyrite, whereas chalcopyrite, over pyrrhotite. Frequently, these sulfides form joint segregations (Figures 2c,d and 9f). Pyrrhotite segregations no more than 0.3 mm in size form intergrowths with pyrite (Figure 9d) or are enclosed in

chalcopyrite (Figure 2c). Chalcopyrite was found to contain inclusions of pentlandite and argentopentlandite $\text{Ag}(\text{Fe,Ni})_8\text{S}_8$ of 10–15 μm in size (Figure 9e, Table 9, No 16, 17).

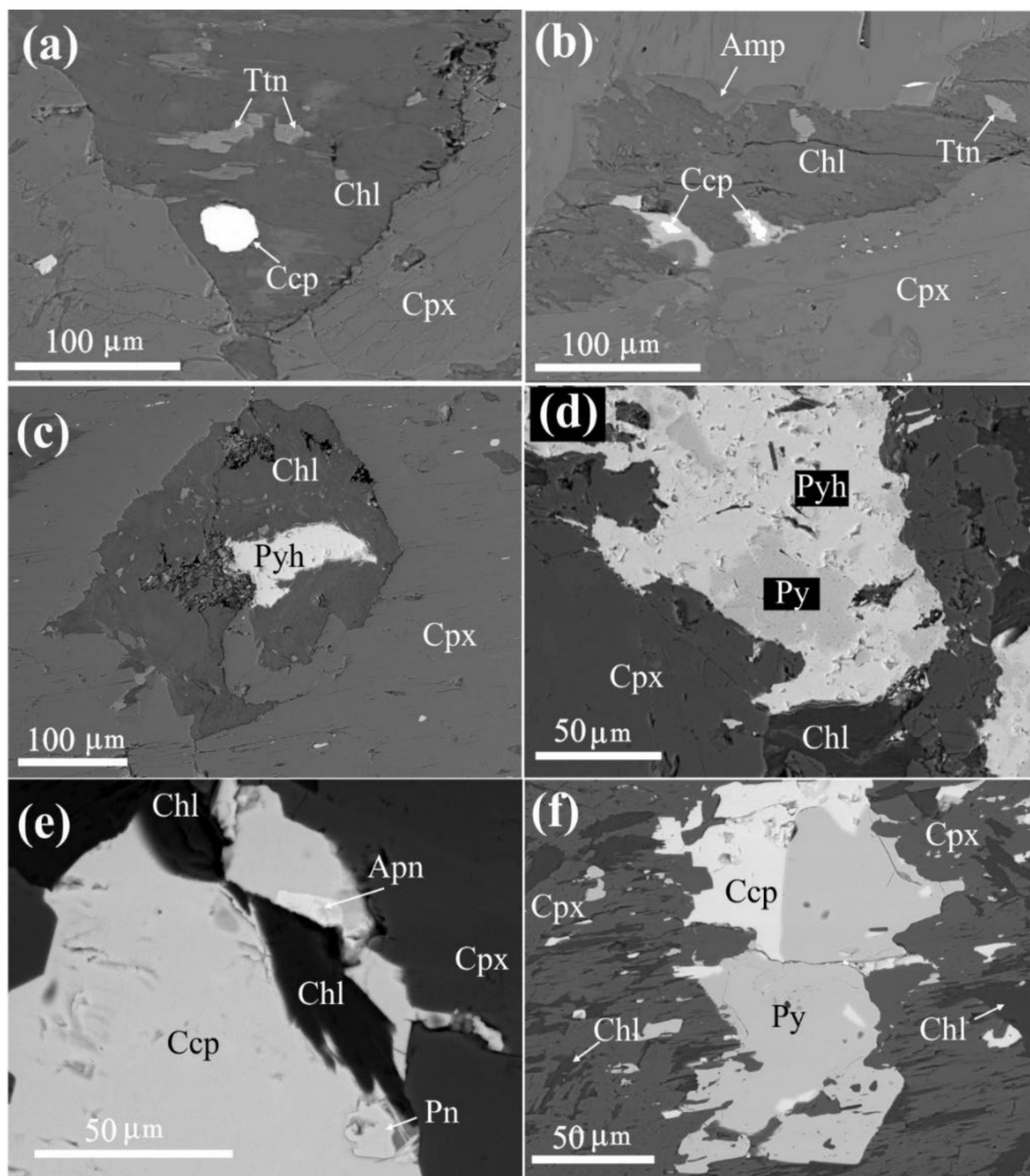


Figure 9. Relationships of sulfide minerals in clinopyroxenites I (a–d) and III (e,f). (a) Interstitial chlorite (Chl) with inclusions of chalcopyrite (Ccp) and titanite (Ttn) in clinopyroxene (Cpx); (b) chlorite veinlets with amphibole rim (Amp) in clinopyroxene. Chlorite contains grains of titanite (Ttn) and partially oxidized chalcopyrite; (c) interstitial chlorite with inclusions of pyrrhotite (Pyh) in clinopyroxene; (d) intergrowth of pyrite (Py), pyrrhotite, and chlorite in clinopyroxene; (e) segregation of chalcopyrite in intergrowth with argentopentlandite (Apn), pentlandite (Pn), and chlorite in clinopyroxene; (f) interstitial segregations of pyrite and chalcopyrite in clinopyroxene. Chlorite develops along the cleavage cracks.

Table 9. Chemical composition of sulfides in clinopyroxenites I–III (in wt.%).

No.	# Sample	Cu	Fe	Ni	Co	S	Ag	Total	Mineral
Pyrite-pyrrhotite-chalcopyrite paragenesis (clinopyroxenite I)									
1	1545-1-33	B.d.	47.61	0.02	0.14	53.24	B.d.	101.01	Py
2	1545-1-43	0.01	47.09	B.d.	0.09	52.68	B.d.	99.87	Py
3	1546-3-3	0.18	45.43	0.05	1.01	51.86	B.d.	98.53	Py
4	1545-2-1	B.d.	62.68	0.05	0.13	37.77	B.d.	100.63	Pyh
5	1545-2-16	0.02	61.4	B.d.	0.13	38.11	B.d.	99.66	Pyh
6	1546-3-1	34.74	30.34	0.01	0.07	33.33	B.d.	98.49	Ccp
7	1546-3-2	34.36	30.72	0.03	0.05	33.31	B.d.	98.47	Ccp
Bornite–chalcopyrite paragenesis (clinopyroxenite II)									
8	101012-36	35.55	29.73	B.d.	B.d.	33.09	B.d.	98.37	Ccp
9	101012-59	35.71	29.29	0.02	0.06	33.03	B.d.	98.11	Ccp
10	101012-35	61.64	11.87	B.d.	0.03	26.14	B.d.	99.68	Bn
11	101012-40	62.25	11.49	B.d.	0.04	24.69	B.d.	98.47	Bn
12	101012-50	61.84	11.45	B.d.	B.d.	25.55	B.d.	98.84	Bn
13	101012-51	70.94	1.04	0.03	B.d.	25.66	B.d.	97.67	Spi-Yar
14	101012-52	68.87	0.99	0.02	0.01	29.72	B.d.	99.61	Spi-Yar
15	101012-60	68.9	1.24	0.05	0.02	29.84	B.d.	100.05	Spi-Yar
Pyrrhotite–chalcopyrite–pyrite (clinopyroxenite III)									
16	211014_1_1	B.d.	34.23	19.1	B.d.	32.71	14.72	100.76	Apn
17	211014_1_4	B.d.	31.49	34.39	B.d.	34.07	B.d.	99.95	Pn
18	211014_2_1	B.d.	60.91	B.d.	B.d.	39.34	B.d.	100.25	Pyh
19	211014_4_3	B.d.	61.33	B.d.	B.d.	38.85	B.d.	100.17	Pyh
20	211014_1_5	34.09	31.05	B.d.	B.d.	35.48	B.d.	100.63	Ccp

Note. spionkopite (Spi), yarrowite (Yar).

Chemical composition of sulfides of various parageneses is given in Table 9. The compositions of pyrite FeS_2 , chalcopyrite CuFeS_2 , and bornite Cu_5FeS_4 are similar to stoichiometric composition for these sulfides. Pyrite in clinopyroxene I contains Co (up to 1 wt.%). The composition of pyrrhotite in pyrite–pyrrhotite–chalcopyrite paragenesis (clinopyroxenite I) corresponds to the formula $\text{Fe}_{0.96-0.97}\text{S}$, whereas pyrrhotite–chalcopyrite–pyrite (clinopyroxenite III), to $\text{Fe}_{0.94-0.95}\text{S}$. Secondary copper sulfide developed mainly on bornite in clinopyroxenite II (Figure 2b) has an intermediate composition between spionkopite ($\text{Cu}_{39}\text{S}_{28}$) and yarrowite (Cu_9S_8) (Table 9, No 13–15). Secondary copper sulfide contains Fe (1–1.2 wt.%).

- Noble metal minerals

Gold, silver, palladium, and platinum minerals are represented by particles to 5 μm , rarely to 10–15 μm in size. They occur predominantly in cleavage cracks in clinopyroxene, less frequently in chlorite or in the interstices of clinopyroxene (Figures 10–12). As the sizes of most particles of noble metal minerals are very small, their chemical composition (Table 10, No 3–14) was determined by ruling out the influence of X-ray excitation of matrix mineral and bringing the sum of measured contents of main minerals to 100%.

Samples of clinopyroxenite 1 with pyrite–chalcopyrite paragenesis (sample 1546) were found to contain particles of palladium antimonides of less than 10 μm , which occur in cleavage cracks in pyroxene (Figure 10a) and chlorite veinlets in it (Figure 10b,c). In chemical composition, palladium antimonides correspond to mertieite I ($\text{Pd}_{11}(\text{Sb,As})_4$) ($\text{Pd}/(\text{Sb} + \text{As}) = 2.72-2.74$) (Table 10, No 1,2) and stibiopalladinite (Pd_5Sb_2) ($\text{Pd}/(\text{Sb} + \text{As}) = 2.33-2.52$) (Table 10, No 3–5). The largest mertieite I grains contain tiny platinum sulfide inclusions 1–2 μm in size (Table 10, No 6).

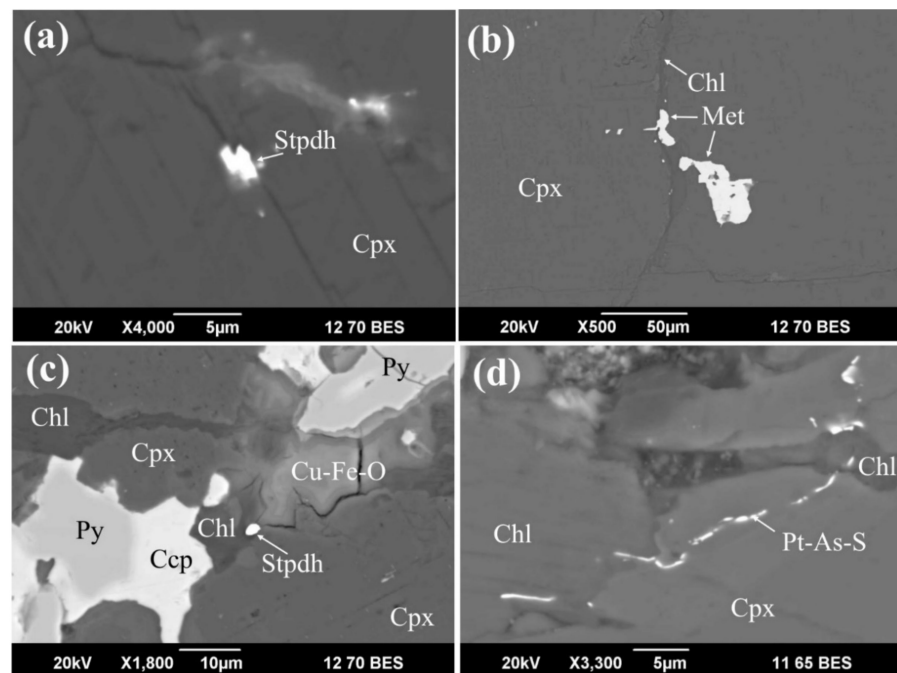


Figure 10. Noble metal minerals in clinopyroxene I. (a) Stibiopalladinite (Stpdn) in the cleavage crack in clinopyroxene (Cpx); (b) mertieite I (Met) grain in clinopyroxene (Cpx) and chlorite (Chl) veinlet; (c) stibiopalladinite (Stpdn) grain enclosed in chlorite. Chlorite is associated with pyrite (Py) and chalcopyrite (Ccp), which are partially replaced by hypergene iron and copper oxides (Fe-Cu-O); (d) veinlets of platinum sulfoarsenide (Pt-As-S) cutting clinopyroxene and chlorite.

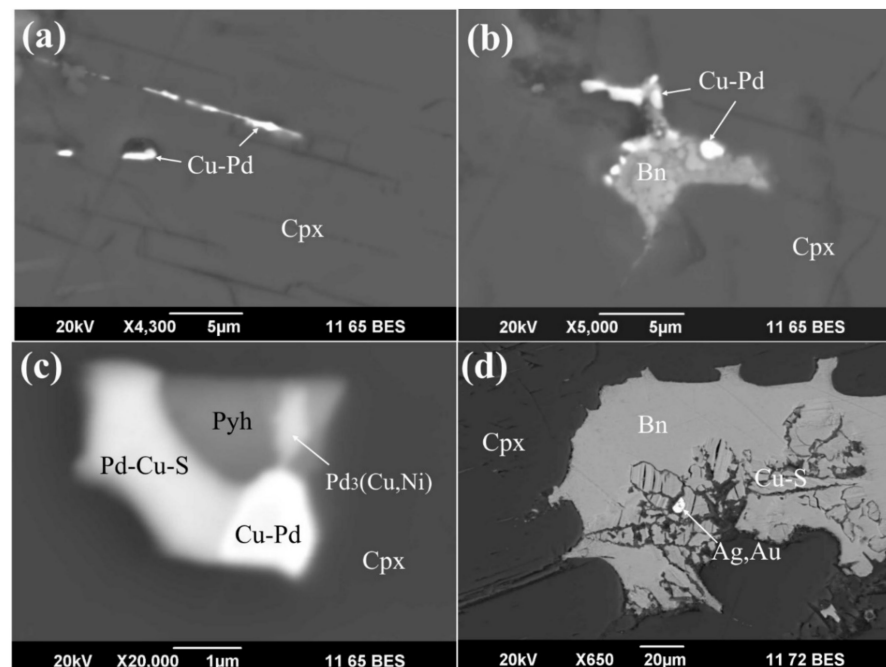


Figure 11. Noble metal minerals in clinopyroxenite II: (a) native copper–palladium phases (Cu-Pd) in cleavage cracks in clinopyroxene (Cpx); (b) interstitial bornite (Bn) segregation in intergrowth with native copper–palladium phases (Cu-Pd); (c) polyphase intergrowth of native Cu-Pd phases (Cu-Pd) (Table 10, No 10), palladium sulfide (Pd-Cu-S) (Table 10, No 12), phases Pd₃(Cu,Ni) (Table 10, No 11) and pyrrhotite (Pyh) in clinopyroxene (Cpx); (d) Au,Ag particle (Table 10, No 13) in secondary copper sulfide (Cu-S) developed on bornite (Bn).

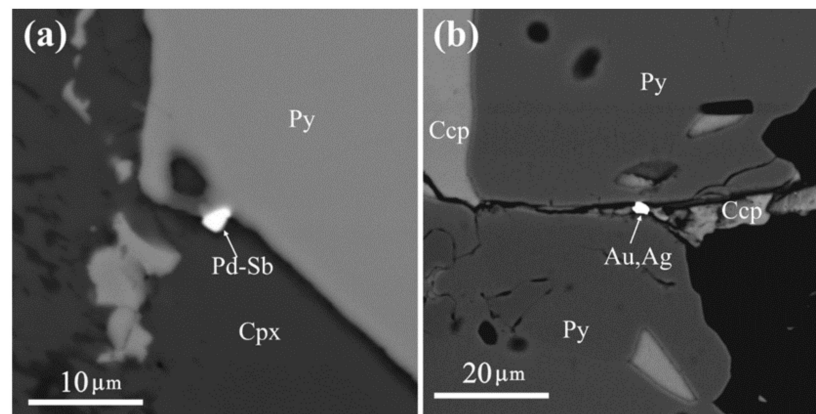


Figure 12. Noble metal minerals in clinopyroxenite III. (a) Crystals of palladium antimonide (Pd-Sb) on the surface of pyrite grain (Py); (b) Ag-Au particle (Au,Ag) (Table 10, No 14) in chalcopyrite (Ccp) at the contact of two pyrite (Py) grains.

Table 10. Chemical composition of noble metal minerals in clinopyroxenites (in wt.%).

No	# Grain	Pd	Cu	Fe	Ni	Pt	Au	Ag	As	Sb	S	Σ	Mineral
1	1546-2-65	71.57	B.d.	0.06	B.d.	0.04	B.d.	B.d.	2.95	25.07	0.02	99.71	Met-I
2	1546-2-66	71.71	B.d.	0.1	B.d.	0.5	B.d.	B.d.	3.01	25.24	0.03	100.59	Met-I
3	1546-2-107	67.20	0.54	1.16	B.d.	B.d.	B.d.	B.d.	3.86	27.24	B.d.	100	Stpdn
4	1546-2-116	69.67	B.d.	0.72	B.d.	B.d.	B.d.	B.d.	4.3	25.30	B.d.	100	Stpdn
5	1546-2-121	67.7	B.d.	0.85	B.d.	B.d.	B.d.	B.d.	4.22	27.23	B.d.	100	Stpdn
6	1546-2-130	50.73	13.77	21.89	B.d.	B.d.	B.d.	B.d.	1.24	4.01	20.76	100	Pd-Fe-S phase
7	1546-3-16	B.d.	B.d.	B.d.	B.d.	51.65	B.d.	B.d.	45.34	B.d.	3.02	100	Spy
8	1546-3-18	B.d.	B.d.	B.d.	B.d.	51.58	B.d.	B.d.	44.91	B.d.	3.52	100	Spy
9	101013-93	57.38	30.41	2.99	B.d.	3.97	5.25	B.d.	B.d.	B.d.	B.d.	100	Skg
10	101013-99	46.52	31.51	8.24	B.d.	2.13	11.6	B.d.	B.d.	B.d.	B.d.	100	Phase Cu > Pd >> Fe
11	101013-100	83.53	9.98	B.d.	6.49	B.d.	B.d.	B.d.	B.d.	B.d.	B.d.	100	Phase Pd ₃ (Cu,Ni)
12	101013-101	68.05	12.42	5.42	B.d.	B.d.	B.d.	B.d.	B.d.	B.d.	14.11	100	(Pd,Cu,Fe) ₂ S
13	101012-154	B.d.	B.d.	B.d.	B.d.	B.d.	16.6	83.4	B.d.	B.d.	B.d.	100	Ag
14	211015_4-1	B.d.	B.d.	B.d.	B.d.	B.d.	70.36	27.53	B.d.	B.d.	B.d.	97.89	Au

Note. Samples of clinopyroxenites I (No 1–8), II (No 9–13), and III (No 14).

Clinopyroxene I also contains the thinnest microveinlets of sulfoarsenide Pt with composition intermediate between sperrylite (PtAs₂) and platarsite (PtAsS) (Table 10, No 7, 8). These microveinlets cut clinopyroxene and are developed along the cleavage cracks of chlorite (Figure 10d).

In clinopyroxenite II with bornite-chalcopyrite sulfide paragenesis, particles of noble metal minerals 3 μm and less in size are also developed in the interstices of clinopyroxene and along its cleavage cracks. They are represented by native Pd-Cu and Pd-Cu-Ni phases (Figure 11,a,b), native gold (kustelite) (Figure 11d), and copper-palladium sulfide. Native and sulfide phases can form polyphase aggregates of grains (Figure 11c). The composition of native Cu-Pd phases is described by the generalized formula Pd_{0.38–0.48}Cu_{0.43}Fe_{0.04–0.13}Au_{0.02–0.05}Pt_{0.01–0.02} (Table 10, No 9, 10), corresponding in stoichiometry to skaergaardite (PdCu). Phase Cu-Pd-Ni (Table 10, No 11) is calculated for the stoichiometry of Pd₃(Cu,Ni) phase which has not been described in literature. The composition of Ag-Au particles (Ag_{0.76–0.90}Au_{0.1–0.24}) corresponds to fineness 170–240‰. The composition of copper-palladium sulfide is calculated for the formula of (Pd,Cu,Fe)₂S not described in literature (Table 10, No 12).

In clinopyroxenite III with pyrrhotite-chalcopyrite-pyrite paragenesis, noble metal minerals are rare, their sizes do not exceed 2–3 μm. Among these minerals, we detected Pd-Sb phases, which in the ratios of components are similar to stibiopalladinite and mertieite, and native gold (see Table 10, No 14). Pd-Sb phases are localized on the surface of large pyrite grains in contact with chlorite developed on clinopyroxene (Figure 12a). A particle of native gold (fineness ~720‰) is enclosed in chalcopyrite at the contact of two pyrite grains (Figure 12b).

4.2. Sulfur Isotopic Composition of Sulfides

Sulfur of pyrite, bornite, and chalcopyrite from clinopyroxenite II and III samples of the Ozernoe occurrence has a homogenous isotopic composition $\delta^{34}\text{S} = -2.1 \dots -2.9$ (Table 11). The $\delta^{34}\text{S}$ values of bornite and chalcopyrite, which compose lattice-like aggregates and replace copper sulfides (spionkopite–yarrowite), virtually do not differ (Figure 13a,b). Table 11 shows the data on the sulfur isotopic composition of sulfides from the Baronsky occurrence—the typical object of gold–palladium mineralization in the Urals. The $\delta^{34}\text{S} = -1.2 \dots -2.6\text{‰}$ values of chalcopyrite from this occurrence (Figure 13e,f) are identical to the sulfur isotopic composition of clinopyroxenite II and III samples from the Ozernoe occurrence.

Table 11. Isotopic composition of sulfur ($\delta^{34}\text{S}$) sulfides from the Ozernoe and Baronsky deposits.

Deposit	Mineral (Number of Analyses)	$\delta^{34}\text{S}$ (VCDT), ‰
Ozernoe, clinopyroxenite II	Chalcopyrite (3)	$-2.3 \dots -2.6$
	Bornite (1)	-2.1
	Bornite, chalcopyrite (4)	$-2.1 \dots -2.6$
	Sulfur sulfides (spionkopite–yarrowite) (4)	$-0.8 \dots -2.7$
Ozernoe, clinopyroxenite III	Pyrite (5)	$-2.1 \dots -2.5$
	Chalcopyrite (5)	$-2.5 \dots -2.9$
Baronsky	Chalcopyrite (7)	$-1.2 \dots -2.6$

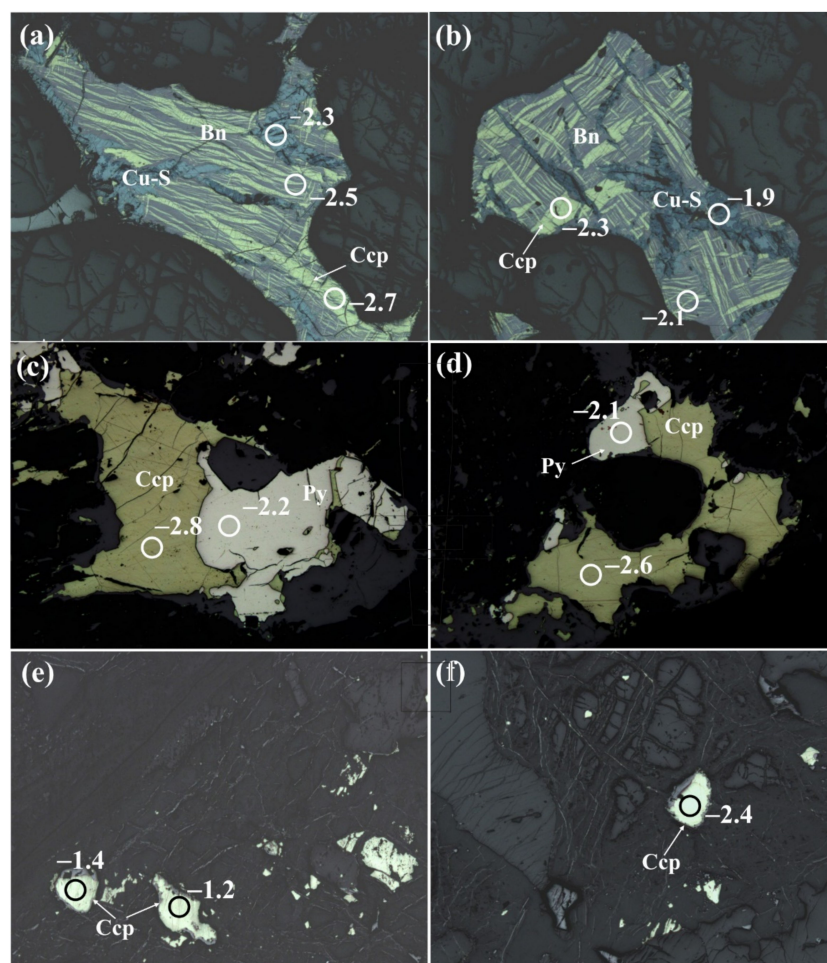


Figure 13. Sulfur isotopic composition of sulfides from Ozernoe (a–d) and Baronsky (e,f) deposits. Sites of analysis are shown by circles with a diameter 100 μm , numbers show $\delta^{34}\text{S}$ values in ‰. Minerals: Py—pyrite, Ccp—chalcopyrite, Bn—bornite, Cu-S—copper sulfide replacing bornite.

5. Discussion

5.1. Sequence of Mineral Formation at Ozernoe Occurrence

Our data show that the primary minerals of the magmatic stage include the main minerals of studied rocks—clinopyroxene, olivine, and Cr-Ti-V-bearing magnetite (with platelets of ilmenite). Interstitial amphibole (magnesian-ferri-hornblende), which was later replaced by chlorite, could have also been deposited from residual fluid-enriched melt (Figure 6c). Further hydrothermal-metasomatic mineral formation proceeded in the interstitial space and along cleavage cracks of clinopyroxene, contacts of clinopyroxene and olivine and microcracks that cut olivine and clinopyroxene. It started from the deposition of amphibole (actinolite and magnesian-hornblende) and bornite-chalcocopyrite solid solutions (iss), which decomposed later. As the temperature decreased and water activity increased, the earlier deposited minerals were replaced by serpentine (on olivine), amphibole (tremolite), secondary magnetite, and chlorite with synchronous titanite. At the contact zone of olivine and clinopyroxene, symplectic aggregates of magnetite with tremolite serpentine were deposited.

The bornite–chalcocopyrite solid solution (iss) in clinopyroxene II is the earliest sulfide. This is supported by its further decomposition into a lattice-like aggregate of bornite and chalcocopyrite and partial replacement by tremolite (see Figure 8c). The process of mineral formation in clinopyroxenites of all groups led to the formation of chlorite, sulfide parageneses with pyrite, pyrrhotite, and chalcocopyrite, as well as platinum group minerals and Au-Ag minerals. Geothermometry of chlorite composition shows that the hydrothermal system by that moment had cooled to 250 °C and continued cooling in parallel with a decrease in the iron content of chlorite (Figure 7).

5.2. Specific Features of the Evolution of Mineral Formation in Clinopyroxenites I–III

A common feature of ore-forming clinopyroxenites I–III is the same specific composition of primary minerals represented by diopside, olivine, and Cr-Ti-V-bearing magnetite. All pyroxenites have the same general tendency of replacement of primary rock-forming minerals by secondary with decreasing temperature: a) olivine → serpentine, secondary magnetite, and b) clinopyroxene → amphibole, secondary magnetite → chlorite.

The determined different ratios of clinopyroxene and olivine contents and different chemical compositions of these minerals indicate variability of the composition of initial melts for clinopyroxenites I–III. This variability reflects the primary magmatic stratification of rocks of the Dzelyatyshor massif, which is, according to [10], manifested as alteration of rocks differing in the composition of clinopyroxene and olivine. A direct dependence of the contents of FeO and Al₂O₃ in primary pyroxene revealed for clinopyroxenites under study (Figure 3b) is typical of the clinopyroxenite–gabbro trend of Uralian massifs and is due to cotectic olivine and clinopyroxene fractionation [21].

Postmagmatic clinopyroxene in clinopyroxenite I has an inverse dependence of FeO and Al₂O₃ contents (Figure 3b). The lowest iron content of clinopyroxene in clinopyroxenite III is most likely related to the postmagmatic “discharge” of part of iron into the oxide phase in the form of thinnest platelets along cleavage cracks (Figure 4a).

The identified higher contents of the main indicator elements (Cr, Ti, V, Mn, Al) in primary magmatic magnetite, compared to secondary hydrothermal magnetite, reflect the ratio of concentrations of these trace elements in the magmatic melt and hydrothermal fluid, which was determined for various ore deposits [22,23].

The revealed differences in the mineral composition of clinopyroxenites I–III and the chemical composition of primary minerals are typical of secondary minerals (Table 12). In particular, clinopyroxenites I–III differ in the set of sulfide minerals and their quantitative ratios (Table 1). In clinopyroxenite I with the lowest content of sulfides (less than 0.1%), chalcocopyrite drastically prevails over pyrrhotite and pyrite. The content of sulfides in clinopyroxenite II can reach 0.5%, and intermediate chalcocopyrite–bornite solid solution among them prevails over chalcocopyrite. In clinopyroxenite III, the content of sulfides

in uncommonly high (to 10%). Their main sulfide mineral pyrite predominates over chalcopyrite and pyrrhotite.

Table 12. Comparative characteristics of primary and secondary minerals of various groups of clinopyroxenites.

Minerals	Clinopyroxenite I	Clinopyroxenite II	Clinopyroxenite III
<i>Primary:</i>			
Clinopyroxene 1	Diopside (4.5–7 wt.% FeO)	Diopside (5–6.8 wt.% FeO)	Diopside (0.7–2.2 wt.% FeO)
Olivine	x(Fa) = 0.25–0.26	x(Fa) = 0.28–0.30	x(Fa) = 0.13–0.15
Magnetite 1	Cr-Ti-V-bearing	Cr-Ti-V-bearing	Cr-Ti-V-bearing
<i>Secondary:</i>			
Clinopyroxene 2	Diopside (9.6–14.5 wt.% FeO)		
Amphibole	Actinolite, magnesio-ferri-hornblende, tremolite	Magnesio-hornblende, tremolite	
Chlorite	Pennine, picnochlorite	Pennine	Pennine
Serpentine	Serpentine A	Serpentine A	Serpentine B
Magnetite 2	0.n wt.% TiO ₂ и MgO	<1 wt.% Cr ₂ O ₃ , MgO, V ₂ O ₃ (Bn-Ccp) _{ss} >Ccp; δ ³⁴ S = −2.1 ... −2.7‰	0.n wt.% MnO
Sulfides	Ccp >> Po > Py		Py > Ccp >> Po; δ ³⁴ S = −2.1...−2.9‰
Pyrrhotite	N _{FeS} = 0.96–0.97		N _{FeS} = 0.94–0.95
Noble metal minerals	Antimonides Pd (mertieite, stibiopalladinite), sulfo-arsenide Pt (sperrylite-platarsite)	Native Pd-Cu and Pd-Cu-Ni phases, native silver (170–240‰).	Mertieite, stibiopalladinite, argentopentlandite, native gold (720 ‰)

Noble metal minerals in clinopyroxenes under study were deposited simultaneously with chlorite. Only platinum sulfoarsenide in clinopyroxene I developed later than chlorite, being deposited in the cleavage cracks of this mineral (see Figure 10d). At the same time, whereas clinopyroxenite II contains native Pd, clinopyroxenites I and III include Pd antimonides. Au-Ag particles of solid solutions detected in clinopyroxenites II and III do not contain palladium (Table 10).

5.3. Association of Noble Metal Minerals at Ozernoe Occurrence

Our study is based on the limited number of samples with gold–palladium mineralization, as a result of which we detected a limited number of noble metal minerals. It was reported in previous works [8,10] that in rocks with a low content of sulfides (no more than 1%), chalcopyrite–bornite segregations similar to those described in clinopyroxenites II are most common. At the same time, some samples contain cubanite, platelets of which can be considered exsolution products of intermediate cubanite–chalcopyrite solid solution. As we did not observe the joint occurrence of bornite–chalcopyrite and cubanite–chalcopyrite segregations, two ore mineral associations were identified—cubanite–pentlandite–pyrrhotite–chalcopyrite and bornite–chalcopyrite [10]. The sets of noble metal minerals in the composition of these mineral associations are virtually the same and consist of native metals, sulfides, antimonides, arsenides, arsenoantimonides, and tellurides (Table 13).

5.4. Features of Native Gold Composition

It was reported in previous research [8,10], which is not in conflict with our data (Table 10), that the composition of native gold in the studied occurrence demonstrates considerable variability. The chemical composition of native gold reported by these authors was recalculated and is presented in Table 14. Some analyses indicate low total contents of elements, which can be due to the small sizes of gold grains and X-ray excitation of matrix minerals. Nevertheless, we present these analyses in the table to demonstrate the ratios

of main components and minimum levels of palladium contents in native gold. From the analyses reported in [10] we excluded those with high contents (more than 1 wt.%) of As, Te, and S elements that are not typical of native gold. In Table 14, analyses of gold grains are grouped based on their association with copper sulfides (bornite, chalcopyrite) and arsenides, antimonides, and tellurides of noble metals.

Table 13. Noble metal minerals at Ozernoe occurrence from [8,10].

Classes	Minerals Associations	
	Cubanite-Pentlandite-Pyrrhotite- Chalcopyrite	Bornite-Chalcopyrite
Native metals	Au-Ag solid solution, tetra-auricupride Au-Cu, auricupride Cu ₃ Au, nielsenite Cu ₃ Pd, native Pt	Au-Ag solid solution, auricupride, skaergaardite *, phase Cu > Pd >> Fe *, phase Pd ₃ (Cu,Ni)*
Sulfides	Vysotskite PdS, braggite (Pt,Pd)S	Phase (Pd,Cu,Fe) ₂ S *
Arsenides	Sperrylite PtAs ₂ , arsenopalladinite Pd ₈ As _{2.5} Sb _{0.5} , atheneite (Pd,Hg) ₃ As, isomertieite Pd ₁₁ Sb ₂ As ₂ , majakite PdNiAs	Sperrylite PtAs ₂ , atheneite (Pd,Hg) ₃ As
Antimonides	Stibiopalladinite (Pd _{5+x} Sb) _{2-x}	Stibiopalladinite (Pd _{5+x} Sb) _{2-x} , mertieite Pd ₅ Sb ₂
Tellurides	Merenskyite PdTe ₂ , moncheite PtTe ₂	Kotulskite PdTe, hessite Ag ₂ Te
Tellurobismuthides, bismuthides	Michenerite PdBiTe, froodite PdBi ₂	Froodite PdBi ₂ , sobolevskite PdBi

Note. *—minerals described in this work in the composition of bornite–chalcopyrite paragenesis.

Table 14. Chemical composition of native gold at Ozernoe occurrence from [8,10].

#	Mineral	Au	Ag	Cu	Pd	Fe	Σ	Fineness, ‰
S (Bornite-chalcopyrite)								
509019	AuCu	74.62	0	23.96	0	0.84	99.42	751
509019	AuCu	74.03	0.94	24.43	0	0.9	100.30	738
509019	Cu ₃ Au	52.2	0	45.71	0	1.65	99.56	524
509019	AuCu	73.85	0	24.33	0	1.36	99.54	742
509019	AuCu	73.17	0	23.96	0	2.28	99.41	736
509019	AuCu	74.03	0	24.93	0	1.17	100.13	739
509019	AuCu	75.27	0	21.01	0	2.1	98.38	765
509019	AuCu	69.3	6.15	21.2	0	3.23	99.88	694
509019	AuCu	69.61	4.38	22.46	0	3.42	99.87	697
509019	ss(Ag,Au,Cu)	50.59	41.66	2.4	0	1.26	95.91	527
509019	ss(Ag,Au,Cu)	55.87	40.71	1.27	0	1.32	99.17	563
509019	ss(Ag,Au,Cu)	49.42	45.93	1.53	0	1.4	98.28	503
509019	ss(Ag,Au,Cu)	46.48	49.07	3.5	0	1.4	100.45	463
509019	ss(Ag,Au,Cu)	48.09	42.51	3.89	0	0.87	95.36	504
509019	ss(Ag,Au,Cu)	27.34	69.25	3.97	0	0.63	101.19	270
509019	ss(Ag,Au,Cu)	27.28	69.11	3.97	0	0.63	100.99	270
509019	ss(Ag,Au,Cu)	30.49	65.89	4.2	0	0.89	101.47	300
509019	ss(Ag,Au,Cu)	33.26	62.86	5.76	0	0.98	102.86	323
S-Te-Sb (bornite, chalcopyrite, mertieite, merenskyite, moncheite, native Te)								
1	ss(Au,Cu,Ag,Pd)	58.9	5.5	17.3	2.8		84.50	697
2	ss(Au,Cu,Ag,Pd)	61.2	6.4	18.5	3.2		89.30	685
3	ss(Au,Cu,Ag,Pd)	55.5	2.5	29.3	1.6		88.90	624
4	ss(Cu,Au,Pd)	49.7	0	38.2	3.8		91.70	542
5	ss(Cu,Au,Ag)	44.7	8.3	41.3	0		94.30	474
6	ss(Cu,Au,Pd)	44.3	0	54	2.1		100.40	441
7	ss(Cu,Au,Pd,Ag)	39.7	1.3	53.5	6		100.50	395
8	ss(Cu,Pd,Au,Ag)	7.9	1.4	63.5	16.4		89.20	89
9	ss(Cu,Pd,Au)	5.5	0	64.3	16.2		86.00	64
10	ss(Cu,Pd,Au,Ag)	9.1	2.2	65.7	16.9		93.90	97

Table 14. Cont.

#	Mineral	Au	Ag	Cu	Pd	Fe	Σ	Fineness, ‰
S-Te-As-Sb (bornite, chalcopyrite stibiopalladinite, kotulskite, braggite, moncheite, atheneite, majakite, mertieite)								
145042	AuCu	66.63	1.54	24.48	4.73	1.58	98.96	673
126010	ss(Au,Ag,Pd)	63.84	17.02	0.00	13.80	1.60	96.26	663
145042	ss(Ag,Au,Cu,Pd)	47.83	44.06	3.84	1.25	1.26	98.24	487
510015	ss(Ag,Au,Pd)	33.49	64.84	0	1.4	0	99.73	336
11	ss(Ag,Au,Cu,Pd)	14.6	80.7	1.2	1	97.50	150	150
12	ss(Ag,Au,Cu)	15.9	83.3	0.9	0	100.10	159	159
13	ss(Ag,Au,Cu)	34.6	62.7	0.8	0	98.10	353	353

Note. ss—solid solution.

In general, native gold at the Ozernoe occurrence is represented by Cu-bearing Au-Ag solid solutions (Cu to 6.5 wt.%) as well as Au-Cu solid solutions and intermetallides (tetraauricupride and auricupride) with wide variations in fineness (150–750‰). According to the composition of components, it belongs to Au-Cu, Au-Cu-Pd, Au-Ag-Cu, Au-Ag, Au-Ag-Pd, and Au-Ag-Cu-Pd. Gold grains containing no palladium are quantitatively predominant (21 grains of the 35 studied). The absence of palladium in the composition of both Au-Ag, and Au-Cu phases was reported in [10] for sample 509019, in which palladium minerals were not detected and native gold is associated with chalcopyrite and bornite. In the samples, which contained sulfides, tellurides, antimonides, and palladium arsenides, native gold is predominantly palladium-bearing. On the whole, there is a tendency to increase the palladium contents in the series—Au-Ag solid solutions (no more than 1.5 wt.% Pd) and Au-Cu intermetallides—Au-Cu solid solutions (to 6 wt.% Pd) and Cu,Pd,Au solid solutions (16.2–16.9 wt.% Pd) (Figure 14).

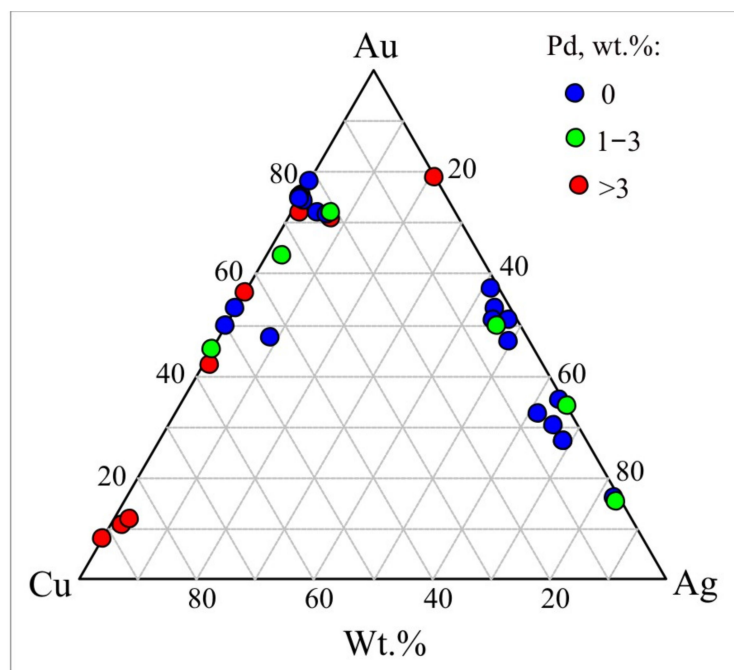


Figure 14. Chemical composition and palladium and copper content of native gold from Ozernoe occurrence on Au-Ag-Cu diagram.

5.5. Reconstruction of Physico-Chemical Parameters of Ore Formation

Following the identified sequence of mineral formation at the Ozernoe occurrence, we determined the stability fields of the main mineral associations and reconstructed the values of

sulfur fugacity in the ore-forming system. $\log f_{S_2}$ – T diagram (modified from [24–26]) shows the stability boundaries of iron, copper, gold, silver, and platinum minerals depending on temperature and sulfur fugacity (Figure 15). Early bornite–chalcopyrite solid solution (iss) in clinopyroxenite II is evidence of high temperatures of formation (350–520 °C). As clinopyroxenite II contains magnetite together with bornite–chalcopyrite solid solution (iss), this allows estimation of temperatures and sulfur fugacity in the system. The stability lines of magnetite (Py+Hem)/Mag and solid solution (Bn+Ccp)/iss intersect at 480 °C and $f_{S_2} = 10^{-3}$, therefore, the stability field of solid solution does not exceed the specified values (Figure 15, field 1). Further in the course of mineral formation, sulfide parageneses with pyrite, pyrrhotite, chalcopyrite, platinum group minerals and Au–Ag minerals were deposited at temperatures 150–250 °C (see Table 6). Chalcopyrite, pyrite, pyrrhotite in clinopyroxenite I together with Pt sulfide in the given range of temperatures are stable at $\log f_{S_2} = -23 \dots -11.5$ (Figure 15, field 2). In clinopyroxenite II, native silver (170–240‰) occurs in association with bornite and chalcopyrite, and their stability field is limited by the equilibrium of Uyt/Ag_{0.75}Au_{0.25} and Ccp/(Bn+Pyh) (Figure 15, field 3).

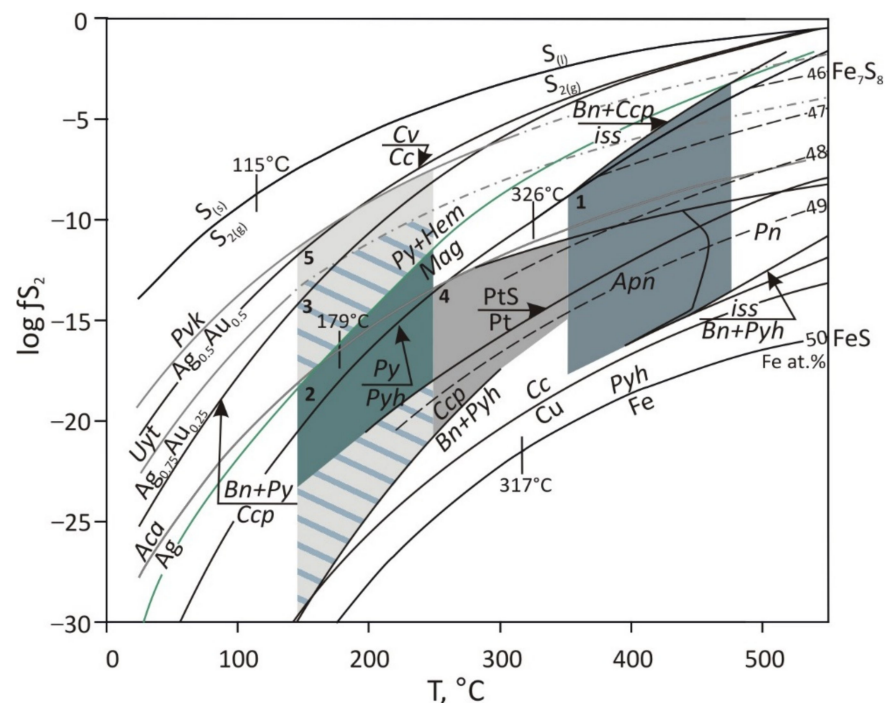


Figure 15. Sulfur fugacity dependence on temperature for Fe–S–O, Cu–Fe–S, Au–Ag–S, and Pt–S systems, and $\log f_{S_2}$ and T estimations for different associations at Ozernoe occurrence. Minerals: Bn—bornite, Ccp—chalcopyrite, iss—bornite–chalcopyrite solid solution, Py—pyrite, Pyh—pyrrhotite, Mag—magnetite, Hem—hematite, Pn—pentlandite, Apn—argentopentlandite, Pvk—petrovskaitite; Uyt—uytenbogaardtite; Aca—acanthite; Cc—chalcocite; Cv—covellite.

In clinopyroxenite III, chalcopyrite grains contain pentlandite and argentopentlandite inclusions. According to the diagram (Figure 15), the stability fields of Ni-bearing phases are located in the higher temperature range. Maximum sulfur fugacity values for this association correspond to the stability line of argentopentlandite ($\log f_{S_2} < -11$), minimum values were estimated from the equilibrium Ccp/(Bn+Pyh) ($\log f_{S_2} > -21$) (Figure 15, field 4). The association native gold (720 ‰) with chalcopyrite, pyrite and pyrrhotite in clinopyroxenite III is stable at $\log f_{S_2} = -30 \dots -7.5$ (Figure 15, field 5).

To estimate the temperatures and values of S_2 fugacity, using a pyrite–pyrrhotite buffer, we analyzed pyrrhotite grains from pyrrhotite–chalcopyrite–pyrite parageneses (clinopyroxenite III). Pyrrhotite composition in this association reaches $N_{FeS} = 0.94–0.95$. The calculations with the help of equations [27,28] showed that during the formation of

pyrrhotite of the given composition, the temperature reaches 196 °C and sulfur fugacity $\log f_{S_2} = -22,7$, which does not go beyond the bounds of the above-estimated boundary values f_{S_2} . The results obtained indicate that mineral formation at the Ozernoe occurrence took place at decreasing temperatures and increased sulfur fugacity in the system.

5.6. Model of Formation of Gold–Palladium Mineralization at Ozernoe Occurrence

The earlier proposed model of formation of gold-palladium Ozernoe occurrence suggests that mineralization is polychronous and polygenic, and formed in three stages [10]. The first, magmatogenic, stage is the concentration of PGE in sulfides and olivine-rich rocks. The second, hydrothermally-metasomatic, stage is a transformation of platinoids into sulfide forms and the enrichment of rocks with gold and copper under the influence of Karshor and Soba plutonites. The third, “epithermal”, stage was marked by the deposition of arsenide, antimonide, and bismuthide forms of platinoids mainly at low-temperature serpentinization and redistribution of gold in the linear zones of concordant tectonic contacts of the clinopyroxenite massif.

In this manuscript we do not discuss the question of the primary magmatic origin of Fe-Cu sulfide melts enriched with native metals in olivine clinopyroxenites of the Dzelyatyshor massif, accepted for the first stage in the model [10], as we did not detect relics of magmatic sulfides in studied samples. The problem of the influence of As, Bi, and Te on the fractionation of Cu, Fe, Ni, and PGE during crystallization of sulfide magma is also beyond [29,30]). At the same time, the role of low-temperature remobilization of non-ferrous and noble metals as well as S, As, Sb, Te, and Bi from magmatic sulfides by post-cumulus fluids, reported in some publications, is undoubtedly important [3,4,31,32]. The most large-scale enrichment of post-cumulus fluids with copper, palladium, and gold takes place on the cooling of melt of gabbro composition. Fluid discharge leads to the formation of high-sulfide mineralization in olivine gabbro, which belongs to the “Volkovsky” type in the Urals [33]. This type of mineralization is represented by large bornite-chalcopyrite bodies with native gold and tellurides of Pd [34].

The conducted research allows us to suggest a simpler model of deposition of gold-palladium mineralization, in which the only source of ore matter and fluid were cooling portions of basic melt. The absence of another external source of substance and fluid is supported by the homogeneity of the sulfur isotopic composition of sulfides and its closeness to the magmatic zero mark. A slight lightening of the sulfur isotopic composition relative to the magmatic zero mark is most likely related to the depletion of heavy isotope during the separation of fluid from basic melt and kinetics of isotope exchange between fluid and sulfides at a further decrease in temperature.

We think that the primary magmatic layering of rocks manifested in different quantitative ratios of clinopyroxene and olivine in them further controls the local trends in the variability of the chemistry of mineral-forming medium and the concentration of ore components, including noble metals, and sulfur in each layer on its cooling.

Copper and iron sulfides as well as noble metal minerals, including native gold, were deposited among the latest and low-temperature minerals. Mineral forms of metals in each portion (layer) of cooled melt were determined by the variability of the activity of post-magmatic fluid components separated from melt. Most likely, these components that bind native metals into their own minerals, when their activity increases, are S, Sb, As, Te, Se, and Bi. The variations in the activity of these components could be due to the change in redox properties of the fluid and concentrations of metal in it, related to the hydration (serpentinization) of olivine. Absorption of water during serpentinization of olivine provided the residual metal-bearing fluid with reducing properties and stability of native forms of metals.

Within the frames of our model, the sets of sulfide minerals and noble metal minerals attributed to earlier distinguished cubanite–pentlandite–pyrrhotite–chalcopyrite and bornite–chalcopyrite mineral associations [10] could also be a result of the evolution of different compositions of the initial melt.

6. Conclusions

- (1) The primary magmatic layering of rocks from the Dzelyatyshor massif, manifested in different quantitative ratios of clinopyroxene and olivine in them, controls the local trends of the variability in the chemistry of the mineral-forming medium and the concentrations of ore components, including noble metals, and sulfur in each separate layer on cooling.
- (2) The deposition of native gold in parageneses with PGM and Cu-Fe sulfides at the Ozernoe occurrence proceeded during the replacement of earlier rock-forming minerals by chlorite. This process terminated mineral formation at the deposit and occurred at temperatures 150–250 °C and high activity of S, Te, Sb, and As of the fluid. The calculated variability in the conditions of mineral deposition during chloritization is reflected in the presence of several sulfide parageneses, in the replacement of native-sulfide forms by arsenide–antimonide forms, in the considerable variability in the iron content of chlorite ($X_{\text{Fe}} = 0.04\text{--}0.43$), and in the sulfur isotopic composition of sulfides.
- (3) Palladium content in native gold increases from Au-Ag solid solution (<1.5 wt.% Pd) to Au-Cu intermetallides—Au-Cu solid solution (to 6 wt.% Pd) and Cu,Pd,Au solid solutions (16.2–16.9 wt.% Pd)
- (4) The sulfur isotopic composition of pyrite, chalcopyrite, and bornite ($\delta^{34}\text{S} = -2.1 \dots -2.9\text{‰}$) just a little lighter relative to the zero mark of deep-seated magmatic sulfur. The deep-seated magmatic basic melt is assumed to be the source of fluid, ore components, and sulfur.

Author Contributions: Conceptualization, V.M. and G.P.; methodology, V.M.; validation, G.P.; investigation, V.M. and T.M.; writing—original draft preparation, V.M.; writing—review and editing, G.P.; visualization, V.M., T.B. and T.M.; Formal analysis, T.B.; supervision, V.M. All authors have read and agreed to the published version of the manuscript.

Funding: The studies are supported by the Russian Foundation for Basic Research (project No. 20-05-00393a) and are carried out as a part of the IGG UB RAS State assignment (state registration No. 122022600107-1), using the «Geoanalitik» shared research facilities of the IGG UB RAS. The re-equipment and comprehensive development of the «Geoanalitik» shared research facilities of the IGG UB RAS is financially supported by the grant of the Ministry of Science and Higher Education of the Russian Federation (Agreement No. 075-15-2021-680). The studies are carried out within the framework of the state assignment of the Sobolev Institute of Geology and Mineralogy of Siberian Branch of Russian Academy of Sciences and of the FRC Institute of Geology Komi SC UB RAS State assignment (state registration No. 1021062211108-5-1.5.2) financed by the Ministry of Science and Higher Education of the Russian Federation.

Data Availability Statement: The data presented in this study are mainly contained within the article and available in the references listed. To a minor degree, the data presented are not publicly available due to privacy and available on request from the corresponding author.

Acknowledgments: We are very grateful to the reviewers for their comments and suggestions.

Conflicts of Interest: The authors declare no conflict of interest.

References

1. Zoloev, K.K.; Volchenko, Y.A.; Koroteev, V.A.; Malakhov, I.A.; Mardirosyan, A.N.; Khrypov, V.N. *Platinum-Metal Mineralization in the Geological Complexes of the Urals*; Department of Natural Resources for the Ural Region: Yekaterinburg, Russia, 2001; 199p. (In Russian)
2. Maier, W.D.; Barnes, S.-J.; Gartz, V.; Andrews, G. Pt-Pd reefs in magnetitites of the Stella layered intrusion, South Africa: A world of new exploration opportunities for platinum group elements. *Geology* **2003**, *31*, 885–888. [[CrossRef](#)]
3. Sluzhenikin, S.F.; Yudovskaya, M.A.; Barnes, S.J.; Abramova, V.D.; Le Vaillant, M.; Petrenko, D.B.; Brovchenko, V.D. Low-sulfide platinum group element ores of the Norilsk-Talnakh camp. *Econ. Geol.* **2020**, *115*, 1267–1303. [[CrossRef](#)]
4. Mansur, E.; Barnes, S.-J.; Ferreira Filho, C.F. The effects of post-cumulus alteration on the distribution of chalcophile elements in magmatic sulfide deposits and implications for the formation of low-S-high-PGE zones: The Luanga deposit, Carajas mineral province, Brazil. *Can. Mineral.* **2021**, *59*, 1453–1484. [[CrossRef](#)]
5. Zaccarini, F.; Anikina, E.; Pushkarev, E.; Rusin, I.; Garuti, G. Palladium and gold minerals from the Baronskoe-Kluevsky ore deposit (Volkovsky complex, Central Urals, Russia) *Mineral. Petrol.* **2004**, *82*, 137–156. [[CrossRef](#)]

6. Anikina, E.V.; Malitch, K.N.; Pushkarev, E.V.; Shmelev, V.R. The Nizhny Tagil and Volkovsky massifs of the Uralian Platinum Belt, and related deposits. In *Field Trip Guidebook. 12th International Platinum Symposium*; IGG UB RAS: Yekaterinburg, Russia, 2014; 48p.
7. Anikina, E.V.; Alekseev, A.V. Mineral-geochemical characteristic of gold-palladium mineralization in the Volkovsky gabbro massif (Platiniferous Urals Belt). *Lithosphere* **2010**, *5*, 75–100. (In Russian)
8. Kuznetsov, S.K.; Kotelnikov, V.G.; Onishchenko, S.A.; Filippov, V.N. Copper-gold-palladium mineralization in ultramafic rocks of the Voikaro-Synya massif in the Polar Urals. *Bull. Inst. Geol. Komi Sci. Cent. Ural. Branch Russ. Acad. Sci.* **2004**, *5*, 2–4. (In Russian)
9. Kuznetsov, S.K.; Filippov, V.N.; Onishchenko, S.A.; Kotelnikov, V.G. Copper-gold-palladium mineralization in ultrabasic rocks of the Polar Urals. *Dokl. Earth Sci.* **2007**, *414*, 501–503. [[CrossRef](#)]
10. Pystin, A.M.; Potapov, I.L.; Pystina, Y.I.; Generalov, V.I.; Onishchenko, S.A.; Filippov, V.N.; Shloma, A.A.; Tereshko, V.V. *Low-Sulfide Platinum-Metal Mineralization in the Polar Urals*; Ural Branch of the Russian Academy of Sciences: Yekaterinburg, Russia, 2011; 150p. (In Russian)
11. Pystin, A.M.; Potapov, I.L.; Pystina, Y.I. The low-sulfide gold-platinum ore occurrence at the Polar Urals. *Zap. RMO* **2012**, *141*, 60–63. (In Russian with English abstract)
12. Remizov, D.N.; Petrov, S.Y.; Kos'yanov, A.O.; Nosikov, M.V.; Sergeev, S.A.; Grigoriev, S.I. New age datings of gabbroides of the kershor complex (Polar Urals). *Dokl. Earth Sci.* **2010**, *434*, 1235–1239. [[CrossRef](#)]
13. Puchkov, V.N. General features relating to the occurrence of mineral deposits in the Urals: What, where, when and why. *Ore Geol. Rev.* **2017**, *85*, 4–29. [[CrossRef](#)]
14. Warr, L.N. IMA–CNMNC approved mineral symbols. *Mineral. Mag.* **2021**, *85*, 291–320. [[CrossRef](#)]
15. Ignatiev, A.V.; Velivetskaya, T.A.; Budnitskiy, S.Y.; Yakovenko, V.V.; Vysotskiy, S.V.; Levitskii, V.I. Precision analysis of multisulfur isotopes in sulfides by femtosecond laser ablation GC-IRMS at high spatial resolution. *Chem. Geol.* **2018**, *493*, 316–326. [[CrossRef](#)]
16. Velivetskaya, T.A.; Ignatiev, A.V.; Yakovenko, V.V.; Vysotskiy, S.V. An improved femtosecond laser-ablation fluorination method for measurements of sulfur isotopic anomalies ($\Delta 33S$ and $\Delta 36S$) in sulfides with high precision. *Rapid Commun. Mass Spectrom.* **2019**, *33*, 1722–1729. [[CrossRef](#)]
17. Leake, B.E.; Woolley, A.R.; Birch, W.D.; Burke, E.A.J.; Ferraris, G.; Grice, J.D.; Hawthorne, F.C.; Kisch, H.J.; Krivovichev, V.G.; Schumacher, J.C.; et al. Nomenclature of amphiboles: Additions and revisions to the International Mineralogical Association's amphibole nomenclature. *Am. Miner.* **2004**, *89*, 883–887.
18. Morimoto, N.C. Nomenclature of pyroxenes. *Am. Miner.* **1988**, *73*, 1123–1133.
19. Cathelineau, M. Cation site occupancy in chlorites and illites as a function of temperature. *Clay Miner.* **1988**, *23*, 471–485. [[CrossRef](#)]
20. Hey, M.H. A new review of chlorites. *Miner. Mag.* **1954**, *30*, 277–292. [[CrossRef](#)]
21. Fershtater, G.B.; Pushkarev, E.V. Magmatic clinopyroxenites of the Urals and their evolution. *Proc. Acad. Sci. USSR Ser. Geol.* **1987**, *3*, 13–23.
22. Nadoll, P.; Angerer, T.; Mauk, J.L.; French, D.; Walshe, J. The chemistry of hydrothermal magnetite: A review. *Ore Geol. Rev.* **2014**, *61*, 1–32. [[CrossRef](#)]
23. Smagunov, N.; Tauson, V.; Lipko, S.; Babkin, D.; Pastushkova, T.; Belozerova, O.; Bryansky, N. Partitioning and Surficial Segregation of Trace Elements in Iron Oxides in Hydrothermal Fluid Systems. *Minerals* **2021**, *11*, 57. [[CrossRef](#)]
24. Fleet, M.E. Phase equilibria at high temperatures. *Rev. Mineral. Geochem.* **2006**, *61*, 365–419. [[CrossRef](#)]
25. Palyanova, G.A.; Sazonov, A.M.; Zhuravkova, T.V.; Silyanov, S.A. Composition of pyrrhotite as an indicator of gold ore formation conditions at the Sovetskoe deposit (Yenisei Ridge, Russia). *Russ. Geol. Geophys.* **2019**, *60*, 735–751. [[CrossRef](#)]
26. Sorokhtina, N.V.; Zaitsev, V.A.; Petrov, S.V.; Kononkova, N.N. Estimation of formation temperature of the noble metal mineralization of the Kovdor alkaline-ultrabasic massif (Kola Peninsula). *Geochem. Int.* **2021**, *59*, 474–490. [[CrossRef](#)]
27. Lambert, J.M.; Simkovich, J.R.; Walker, P.L. The kinetics and mechanism of the pyrite-to-pyrrhotite transformation. *Metall. Mater. Trans. B* **1998**, *29B*, 385–396. [[CrossRef](#)]
28. Chareev, D.A.; Osadchii, E.G. Pyrrhotite-pyrite equilibria in the Ag–Fe–S system at 245 to 310 °C and standard pressure. *Geochem. Miner. Petrol. Bulgar. Acad. Sci.* **2005**, *43*, 41–46.
29. Sinyakova, E.; Karmanov, N.; Kosyakov, V.; Distler, V. Behavior of Pt, Pd, and Au during crystallization of Cu-rich magmatic sulfide minerals. *Can. Mineral.* **2016**, *54*, 491–509. [[CrossRef](#)]
30. Sinyakova, E.F.; Borisenko, A.S.; Kosyakov, V.I. Effect of the presence of As, Bi and Te on the behavior of Pt metals during fractionation crystallization of sulfide magma. *Dokl. Earth Sci.* **2017**, *477*, 1422–1425. [[CrossRef](#)]
31. Wood, S.A. The aqueous geochemistry of the platinum group elements with applications to ore deposits. In *Geology, Geochemistry, Mineralogy and Mineral Beneficiation of Platinum Group Element*; Cabri, L., Ed.; Canadian Institute of Mining, Metallurgy and Petroleum: Ottawa, ON, Canada, 2002; Special Volume 54, pp. 211–249.
32. Holwell, D.; Adeyemi, Z.; Ward, L.A.; Smith, D.J.; Graham, S.D.; McDonald, I.; Smith, J.W. Low temperature alteration of magmatic Ni-Cu-PGE sulfides as a source for hydrothermal Ni and PGE ores: A quantitative approach using automated mineralogy. *Ore Geol. Rev.* **2017**, *91*, 718–740. [[CrossRef](#)]
33. Poltavets, Y.A.; Poltavets, Z.I.; Nechkin, G.S. Volkovsky deposit of titanomagnetite and copper-titanomagnetite ores with accompanying noble-metal mineralization, the Central Urals, Russia). *Geol. Ore Depos.* **2011**, *53*, 126–139. [[CrossRef](#)]
34. Murzin, V.V.; Palyanova, G.A.; Anikina, E.V.; Moloshag, V.P. Mineralogy of noble metals (Au, Ag, Pd, Pt) in Volkovskoe Cu-Fe-Ti-V deposit (Middle Urals, Russia). *Lithosphere* **2021**, *21*, 643–659. [[CrossRef](#)]